

Semipolar wide-band III–N-layers on a silicon substrate: orientation controlling epitaxy and the properties of structures (review)

© V.N. Bessolov, E.V. Konenkova

Ioffe Institute,
194021 St. Petersburg, Russia
e-mail: lena@triat.ioffe.ru

Received February 20, 2023

Revised May 26, 2023

Accepted July 13, 2023

The experimental results of the recent years on the synthesis of semipolar wide-band III–N-layers on a nanostructured silicon substrate are summarized. The idea of synthesis involves the formation of Si(111) side walls on the silicon surface, then the epitaxial nucleation of the layer in the „c“ direction of the crystal, followed by the fusion of blocks in the semipolar direction of the surface. Examples of orientation controlling epitaxy of semipolar AlN(10–11)-, GaN(10–11)-, GaN(11–22)-layers synthesized on nanostructured Si(100), Si(113) substrates by methods of metalorganic vapor phase epitaxy and hydride vapor phase epitaxy are shown. The review presents a summary and the prospects for further developments in the field of optoelectronics based on the platform — „semipolar GaN on Si“.

Keywords: wide-band semipolar III–N-layers, orientation controlling epitaxy, nanostructured silicon substrate

DOI: 10.61011/TP.2023.09.57354.31-23

Introduction

Studies of III-nitride semiconductors began in 1932 when GaN was first synthesized by interaction of metallic gallium with ammonia (NH₃) at 900–1000°C [1]. In 1969, the hydride vapor phase epitaxy (HVPE) [2] technique was used to deposit GaN on sapphire substrates, and two years later, metalorganic vapour phase epitaxy (MOCVD) [3] was used to grow GaN and AlN. In the early 1980s, Akasaki etc. proposed the so-called two-step layer [4], growth approach, which led to the most important breakthrough in GaN technology.

An important success for the development of GaN-based optoelectronic devices was the growth of GaN *p*-type layers. In 1992 Nakamura proposed a method for producing GaN of *p*-type by thermal annealing of Mg-doped GaN in a nitrogen [5] environment. On the basis of these achievements, the first blue LED with a double InGaN/GaN [6] heterostructure was demonstrated in 1993. Aluminum nitride (AlN) was appreciated in microelectronics in the mid-1980s due to its wide band gap and relatively high thermal conductivity [7] for single-crystals. The basic physical characteristics of InN, with which hopes for its widespread application in electronics and optoelectronics are held out in [8].

Conventional III-nitrides *c*-plane are characterized by spontaneous and piezoelectric polarization due to the lack of inversion symmetry in the crystal structure of wurtzite [9,10].

Interface charges lead to distortions in the energy landscape causing the quantum confined Stark effect (QCSE) [11], increasing the recombination time of charge carriers [12] and decreasing the optical gain [13].

Low quantum efficiency becomes a serious problem for the design of LEDs for green and yellow emission spectra because the active area of the InGaN quantum well requires a much higher fraction of InN and thus the increased strain creates even stronger piezoelectric fields [14,15].

One promising way to overcome the fundamental problems outlined above is to grow InGaN/GaN heterostructures along the semi-polar or nonpolar direction. Such semi-polar and non-polar structures can effectively reduce or eliminate internal electric fields (Fig. 1). For example, electric fields completely disappear on the crystal faces of GaN (11–20) or GaN (11–10). Crystal planes orientated between (0001) and (10–10) (i. e., polar and nonpolar) faces are called „semi-polar“. In these cases, the internal fields decrease as a function of the angle θ of inclination of the semi-polar plane relative to the *c*-plane, for example, the angle of inclination of the GaN plane (11–22) relative to the plane (0001) is $\sim 58^\circ$, whereas the plane GaN (20–21) is inclined by 75° .

Fig. 2 shows the positions of some semi-polar and non-polar planes in GaN [16] crystal, and Fig. 3 shows the polarization induced by piezoelectric fields in the layer for

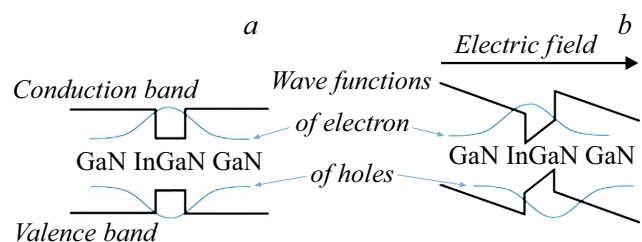


Figure 1. Schematic representation of the zone structure for non-polar (a) and polar (b) InGaN/GaN structures.

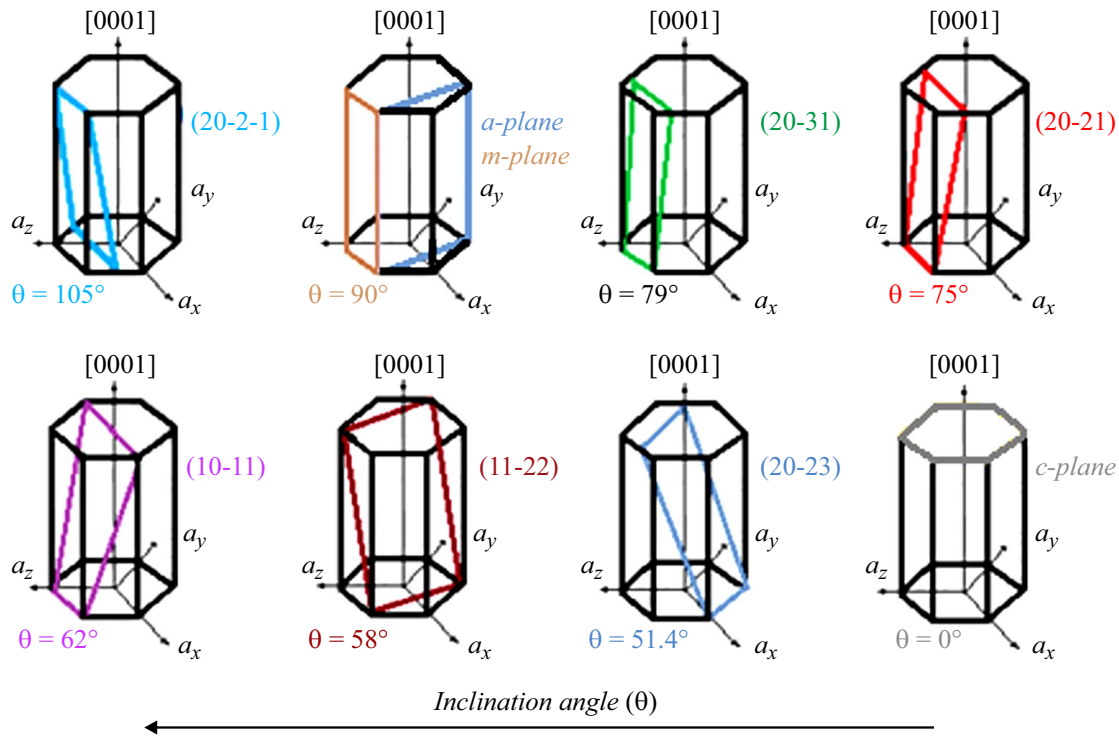


Figure 2. Schematic representation of crystal planes in GaN lattice with different tilt angles (θ) [16].

InGaN/GaN structures with different indium composition as a function of the angle between the semi-polar and GaN(0001)-planes [17].

Early work on semi-polar and nonpolar GaN was mainly devoted to calculations of the longitudinal piezoelectric field of an InGaN/GaN structure as a function of the angle between the polar plane and the (0001) plane. The calculation shows that the piezoelectric field along the $\langle 0001 \rangle$ direction leads to the lowest recombination probability of charge carriers, but the piezoelectric field decreases and the recombination probability increases significantly when the crystal faces are tilted away from the (0001) plane of GaN [18].

Park [19] predicted that the effective hole mass in strained nonpolar InGaN/GaN quantum wells should be smaller than that in strained polar quantum wells, potentially increasing the hole mobility and hence should improve the conductivity of semi-polar *p*-GaN. Clearly, these data indicate that semi-polar or non-polar GaN shows significant potential for the fabrication of optoelectronic devices compared to polar GaN-based emitters.

The first attempt to grow semi-polar GaN layers by MOCVD was demonstrated in 1987 [20], and the synthesis of a non-polar GaN layer on a LiAlO₂ substrate by molecular-beam epitaxy (MBE) [21] was reported in 2000. The great academic and commercial success achieved by growing polar GaN on sapphire, and the potential benefits to be gained by looking at other growth directions, have encouraged scientists to explore the synthesis of semi-polar GaN layers on sapphire and silicon substrates. It was found

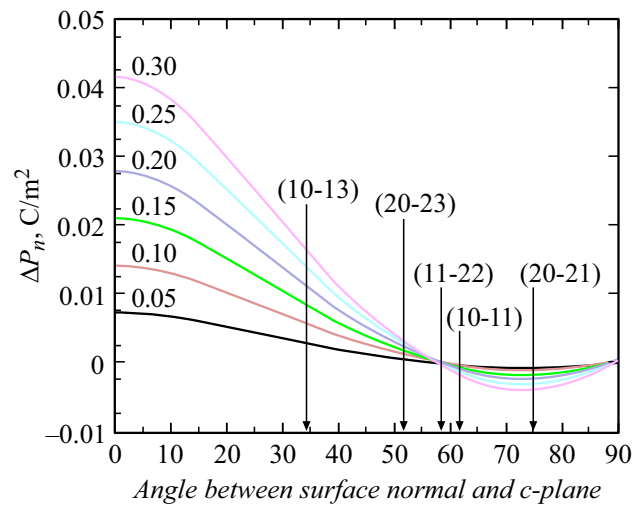


Figure 3. Dependence of the difference of ΔP polarization values at the interface between $\text{In}_x\text{Ga}_{1-x}\text{N}$ ($0.05 < x < 0.3$) on the value of the angle between the semi-polar plane and the (0001) plane. The arrows show the ΔP values for different semi-polar planes [17].

that semi-polar or non-polar GaN can indeed be obtained by growing GaN on sapphire *r*-Al₂O₃ [22] or *m*-Al₂O₃ [23], but it was found that it is difficult to achieve semi-polar or non-polar GaN on any flat Si(100) [24] substrate. Semi-polar layers have been synthesized on sapphire substrates by the classical approach using a high-temperature AlN [25] buffer layer, but the quality of the semi-polar layers is

inferior to that of the polar layers: the width of the X-ray diffraction curves at half maximum (FWHM) is typically $0.2\text{--}0.3^\circ$ for semi-polar GaN layers and only 0.08° for polar GaN when epitaxied on a sapphire substrate

In polar GaN, the stacking faults are confined to the interface between GaN and sapphire and are also perpendicular to the growth direction, while in the synthesis of semi-polar GaN, the stacking faults penetrate the layer in addition to mismatch dislocations. Homo-epitaxial growth is known to give the best performance, so all InGaN/GaN-based semi-polar emitters with the best performance are grown on semi-polar cut gallium nitride [26–30] substrates. These substrates were obtained by growing a polar flat layer of GaN on sapphire up to 10 mm thick by the HVPE method, and then cut, ground, and polished along the semi-polar or non-polar orientation [31,32].

1. Synthesis of layers

1.1. Synthesis of layers on planar substrate

1.1.1. AlN and GaN on Si (111)-substrate

The history of epitaxy of group III-nitride layers on silicon substrate emerged about half a century ago [3], but the main development of this direction began since 1998 [33–36].

Silicon is the preferred substrate material because of its cost-effectiveness [37], large size, excellent thermal stability [38], and high thermal conductivity ($142\text{ W}/(\text{m} \cdot \text{K})$) [39].

Due to the large lattice mismatch ($\sim 17\%$) and thermal expansion coefficient ($\sim 54\%$) between GaN and Si, it is difficult to grow GaN layers with low dislocation density and without cracks. Another of the difficulties of GaN epitaxy on Si is the chemical reactivity of Si with almost all elements at elevated temperatures. The use of certain metals such as, for example, iron or gold in Si technology should be avoided due to their high diffusivity to penetrate Si and further form deep traps that degrade device properties. Gallium forms a eutectic with silicon at room temperature [40], and this alloy is very destructive because once formed, it continues to grow, fed by epitaxial layers which it destroys [37].

It is found that there is a parasitic reaction of Ga with silicon in the MOCVD epitaxy process through a thin buffer layer AlN (Ga melting etching) [41,42], and the low mobility of Al adatoms on both the silicon and aluminium nitride surfaces hinders the structural rearrangement of adatoms and makes the surface morphology of the AlN epitaxial film rough [43].

Various technological approaches have been successfully applied to improve the quality of GaN layers during epitaxy on silicon substrates: firstly, the synthesis of low-temperature and high-temperature intermediate AlN [44] layers, and secondly, the formation of buffer AlN/GaN super-lattices. AlN/GaN superlattice technology can effectively control the stress and improve the crystal quality, and the large lattice mismatch between GaN, AlN and Si can be reduced [45]. Vertically propagating dislocations can be

terminated at superlattice interfaces, which consequently improves crystal quality. Using these methods, the authors [46] reported the growth of GaN-on-Si(111)-transistors with high electron mobility (HEMTs).

The method of growing GaN layers on a sapphire substrate with an intermediate low-temperature AlN [47] layer was also applied to the growth of GaN on a Si [48] substrate. Note that the crystal quality and residual stresses in epitaxial GaN layers on Si still cannot be comparable to those of GaN layers on SiC [49] substrate. In GaN synthesis, it is found that there is a change in the surface potential in the layer due to defects that act as deep acceptors [50].

The first light generation effect of III-nitride semiconductor materials grown on GaN nano-prisms deposited on silicon substrates was reported in [51]. The generation obtained on epitaxial GaN layers grown on S(111) substrates is described in [52].

In 2009 it was possible to grow a GaN-based laser structure with a waveguide on a Si(111) [53] substrate.

In 2016 monolithic integration of GaN-based LEDs with vertical field-effect transistors on sapphire [54] was reported. InGaN/GaN-based GaN-on-Si, quantum-sized InGaN/GaN devices with different functionalities are reported [55–61]. Orientation-controlled epitaxy of GaN layers on a Si(111) substrate was demonstrated using a very thin Al_2O_3 layer that controlled the orientation of AlN [62] seed layers. An anisotropic model for stresses due to thermal mismatch between film and substrate in gallium nitride and aluminium nitride films grown on Si(111) substrates is published in [63]. The authors determined the stresses in the layers by Raman light scattering spectral curve frequency shifts and observed good agreement with the model for polar layers of III-nitrides.

1.1.2. AlN and GaN on Si(100)-substrate

The use of Si(100) as a substrate for the epitaxy of III–N semiconductor layers is preferred because of the possible integration of gallium nitride and silicon electronics. Attempts to synthesize hexagonal III-nitride layers on a Si(100) substrate have shown that, in contrast to the Si(111) substrate, the process results in a low-quality structure. This is due primarily to the fact that the synthesis of hexagonal structure of III-nitrides on the planar cubic structure of Si(100), firstly, the layers of 6-tot-point symmetry are born on the surface of with 4-tot-point symmetry with a large difference in the constant lattice and, secondly, at the mismatch of crystal symmetry layers grow in two crystal-lattice orientations. It is known [64] that AlN layers are formed on the Si(100) substrate in the form of columnar domains. This result is not surprising since Si(001) and AlN(0001) are known to have a large difference of permanent lattices and different crystallographic symmetry of the [65] planes. It is also known that the synthesis of AlN and GaN on Si(100) leads to polycrystalline or textured layers, at least with very rough surfaces, consisting of many grains [66]. Usually, Si(100) substrates disoriented in the $\langle 110 \rangle$ to $4\text{--}7^\circ$ direction

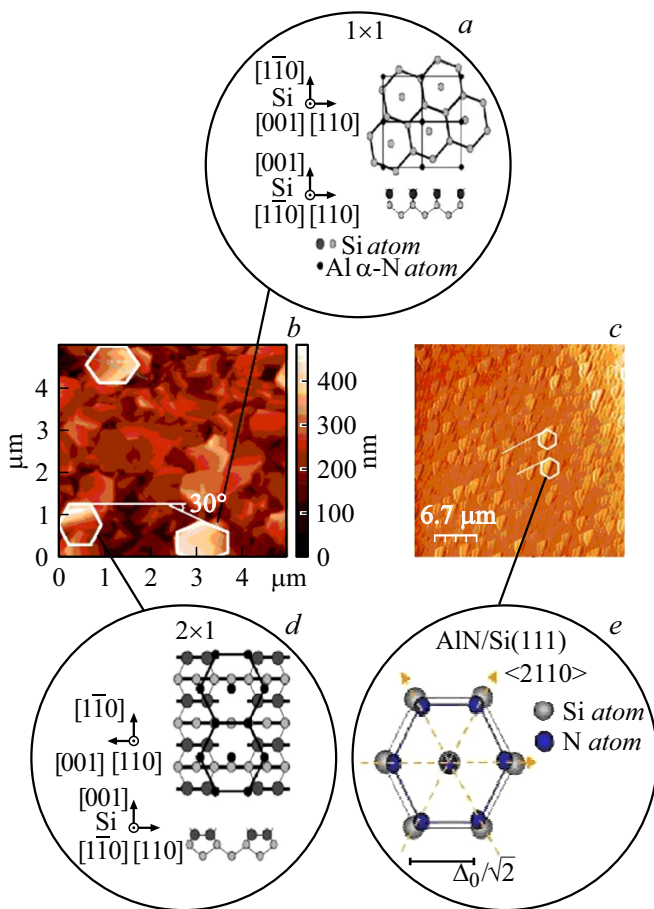


Figure 4. Schematic representation of AlN interfaces on Si(1×1) (a), Si(2×1) (d) and Si(111) (e) and AFM scan images of AlN(0001) surfaces on Si(100) (b) substrates and Si(111) (c) [74].

are used to improve the quality of hexagonal AlN layers, but disoriented Si(100)-substrates are not applicable in silicon microelectronics technology because it is difficult to form a reproducible surface microrelief that has the necessary characteristics [67].

In the studies on the synthesis of AlN, GaN on Si(100) substrates, AlN was synthesized by MBE [68], magnetron sputtering [64], HVPE [69], and GaN with aluminium nitride buffer layer was synthesized by laser deposition [70], MBE [71], HVPE [72] and MOCVD [73].

The HVPE method was used to elucidate the possibility of synthesizing AlN and GaN on Si(100) and for comparison on Si(111)-substrates, which were pre-treated in ammonium sulfide solution to remove the natural oxide. The epitaxy temperature in hydrogen atmosphere of AlN layers was 1080°C, and GaN — 1050°C.

When the SiO₂ layer chemically interacts with (NH₄)OH, part of the oxide is removed and the sulfide layer is formed, and two types of Si(2×1) and Si(1×1) surface lattices can be formed. The nucleation of AlN on Si(100) with surface

lattice (2×1) and (1×1), will in turn lead to the formation of AlN columnar structures of two orientations (Fig. 4, a, d).

Comparison of atomic-force microscopy (AFM) images of AlN layers synthesized on Si(100) substrates showed that a polycrystalline structure (Fig. 4, c) and a columnar hexagonal structure of AlN on a sulfidized substrate (Fig. 4, b) are formed at the initial growth stage. After treatment of Si(100) in sulfide solution, the formation of pillars mainly of two crystal-lattice orientations — AlN–I and AlN–II (Fig. 4, a, d). AFM image of the surface of the AlN layer synthesized on Si(111) substrate showed that only one type of crystal-lattice orientation — AlN–I (Fig. 4, c, e). The nucleation of an AlN epitaxial layer on a Si substrate depends on the presence of oxides on its surface.

The presence of two columnar AlN nuclei deployed at 30° relative to each other results in a broadening of the X-ray diffraction curve of the GaN/AlN/Si(100) structures compared to the data for the GaN/AlN/Si(111) structures.

1.1.3. GaN(10–13)/Si(100)

Let us consider the results of the synthesis of semi-polar thick GaN layers grown by HVPE on a flat disoriented Si(100)-substrate with an intermediate buffer AlN layer as a simple way to utilize the surface faces of the disoriented Si(100) substrate for the growth of semi-polar [75,76] layers.

During the epitaxy of AlN in hydrogen atmosphere on Si(100) substrate by HVPE method, many individual nucleating seeds of both hexagonal and cubic modifications are formed at the initial stage. At a relatively low growth temperature for AlN ($T = 950^\circ\text{C}$) the layer structure becomes less ordered, but the size of these blocks increases as they grow, but the surface of the AlN layer takes the form of faceted blocks consisting of nanocrystals with planes like c -AlN(111), h -AlN(1102), h -AlN(1012), h -AlN(1013), etc. [77]. The presence of different faceting of AlN nuclei leads to the growth of GaN in different crystallographic directions. X-ray diffraction studies showed that an epitaxial semi-polar GaN(10–13) layer is formed with the half-width of the rocking reflex curve (0004) of the GaN layer of $\omega_\theta = 30$ arcmin value. The effect of crystal faceting of the buffer AlN layer on the structure of the semi-polar GaN layer was demonstrated by Amano et al. [78]. The authors have successfully grown semi-polar GaN(10–13) and GaN(10–15) layers on Si(001) substrates using different faces of AlN layers synthesized by magnetron sputtering using the MOCVD method. The authors [79] have shown that it is possible to synthesize GaN layers with the „ c “ axis tilted at 18°(211) using the MOCVD method.

1.1.4. GaN(20–23)/3C–SiC/Si(100)

Semi-polar layers were synthesized on Si(100) substrate with different surface disorientation (2° , 4° , 7°). In the first step, a SiC nanolayer was formed using the technique described in [80], then an AlN buffer layer with a thickness

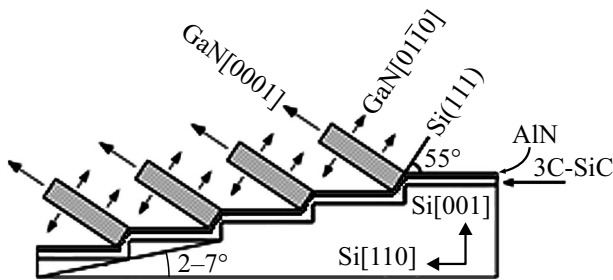


Figure 5. Schematic representation of the synthesis process of semi-polar GaN on 3C–SiC(111)/Si(100) [82].

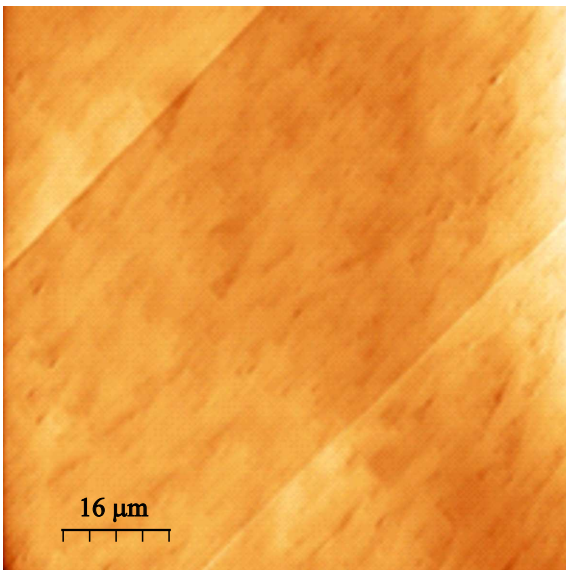


Figure 6. AFM scan image of the surface GaN(20–23)/3C–SiC(111)/Si(100).

of ~ 100 nm, was grown by the HVPE method, and — then — a GaN core layer with a thickness of 10–15 μm in a hydrogen atmosphere by [81].

The X-ray diffraction results of the grown GaN layers unambiguously indicate the presence of GaN(20–23)-layer single-crystal structure, which was synthesized on the formed AlN/3C–SiC faces of the disoriented Si(100) surface (Fig. 5).

The structures exhibited bending and the radii of curvature in the two perpendicular directions were significantly different. AFM of the GaN layer surface showed that the growth „pit“ structures have an asymmetric shape characteristic of epitaxy in the semi-polar direction, and in the $\langle 2110 \rangle$ direction parallel crack lines of the layer are manifested (Fig. 6). The formation of SiC nanocrystalline nuclei in the solid-phase method occurs at very low supersaturation, the so-called chemical affinity [80], which leads to „quasi-equilibrium“ growth of nuclei because the solid-state reaction occurs inside the substrate Si rather than outside. We suggest that in the places where steps are present, due to the disorientation of the (100) plane and

the „of the quasi-equilibrium“ process of hetero-epitaxy, „etching“ of the steps occurs with the formation of Si(111)-substrate faces and simultaneous formation of faces of 3C–SiC(111). It is known that the inclination angle of the GaN(20–23) plane to the GaN(0001) $\sim 51.5^\circ$ plane is close to the angle between the (111) and (100) planes in the cubic lattice 3C–SiC $\sim 55^\circ$, and this is one of the stimuli for the growth of the GaN layer in the inclined direction with respect to the (100) plane (Fig. 5).

Another stimulus for the growth of the GaN(20–23) layer in this particular semi-polar direction is the good agreement of the GaN and 3C–SiC, lattices in at least one of the crystallographic directions. Indeed, if we consider the lattice of semi-polar GaN(20–23) and the lattice of a cubic 3C–SiC, we can see that the GaN(20–23) layers should experience different strain in perpendicular directions. Evaluation of the strain magnitude for gallium nitride layers grown on 3C–SiC(100), showed that in the $\langle 2110 \rangle$ direction, this magnitude $\sim 3.6\%$, and in the $\langle 2023 \rangle$ direction — $\sim 19.8\%$. The authors [83] reported the MOCVD preparation of GaN(20–23) layers of thickness 1.4 μm , grown on 3C–SiC/Si(100) with disorientation 4° towards $\langle 110 \rangle$. In more recent work [84], semi-polar GaN layers with surface orientations of (10–11), (20–23) and (10–12) were obtained. The growth of layers (10–11) was along 3C–SiC/Si(110) and 3C–SiC/Si(–110), while the growth of layers (20–23) and (10–12) was only along 3C–SiC/Si(110). Layers (10–11) had a rough surface morphology, while layers (20–23) and (10–12) had a mirror-smooth surface.

The synthesis of AlN on Si(001) substrate with 3C–SiC, buffer layers, which was obtained by chemical deposition, leads to a complicated structure at the AlN/SiC interface. Hexagonal AlN does not grow directly on 3C–SiC, but first, a cubic AlN of pyramidal shape is nucleated, then when the cubic AlN grows to thickness of 10 nm, the structure of the growing AlN crystal changes to hexagonal type [85,86].

1.1.5. GaN/3C–SiC/Si(210)

The synthesis of semi-polar gallium nitride layers was carried out similarly to the method described in Section. 1.1.4, but the initial silicon substrate had an orientation (210).

In this case, X-ray diffraction studies have shown, that the GaN layer crystallizes in the form of blocks as epitaxial growth proceeds, with the surface orientation of the layer changing as follows:

$$(101-5) \rightarrow (101-4) \rightarrow (101-3) \rightarrow (101-2).$$

The analysis of the oblique symmetric reflex (1124), the half-width of which was 25 arcmin, allows us to make a statement about the epitaxial character of layer growth. Scanning electron microscopy (SEM) of the surface of the layers showed that the layer has a characteristic structure of a blocky layer grown in the semi-polar direction (Fig. 7).

This behavior of the GaN layer during epitaxy on Si(210) can be explained based on a model of layer growth

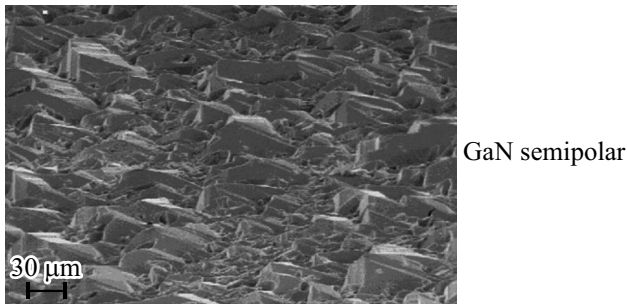


Figure 7. SEM image of the surface of the structure GaN/AlN/3C–SiC/Si(210) [87].

under conditions where, after chemical etching of the substrate, the surface should consist of steps with facets of Si(100), Si(110) and Si(111), which should result in a mosaic silicon carbide surface (3C–SiC(110), 3C–SiC(100), 3C–SiC(111)), and will favor the layer growth in the most favorable direction.

The nucleation of AlN and growth of GaN layers in the semi-polar direction under different facets of 3C–SiC-layer occur in different semi-polar directions [87]. Recently, the authors [88] proposed a model that highlights the possibility of controlling the growth direction of the semi-polar AlN layer by forming a 3C–SiC, for example, in the synthesis of AlN(10–13)/3C–SiC/Si(110).

The use of the faces of the structured substrate to control the crystallographic structure of the semi-polar layer is displayed in [78,89]. The application of directional AlN deposition in the magnetron sputtering technique is a promising method to obtain semi-polar GaN layers on Si(100)-substrate [90].

So, it is difficult to grow semi-polar GaN with large tilt angle to c -plane on planar Si substrate due to the lack of compatible epitaxial relationship between semi-polar GaN crystal on any oriented Si substrate. However, given the wide availability of Si substrates and the ease of forming a structured Si surface by either dry or chemical wet etching, it is expected that the growth of semi-polar GaN layers on Si structured substrate will show major advantages over GaN that is grown on a flat substrate.

1.2. Synthesis and properties of layers on nanostructured (NP–Si)-substrate

In order to select compatible Si substrates for epitaxial growth of semi-polar GaN on tilted facets, the crystallographic relationship between the substrate and the desired semi-polar orientation must be considered. In paper [91], the authors noted that to obtain the semi-polar orientation of the structure surface, the angle between the nucleation edge and the substrate surface should be equivalent to the slope between the I c -plane of GaN and the target semi-polar plane. The angles between the silicon planes (hkl) and the surface of silicon wafers of different orientations

Table 1. The angles between the Si(hkl)-planes and the surface of the Si [81] substrate.

Si-planes			The angles between the Si(hkl) and above the planes of the substrate of different orientations			
h	k	l	(100)	(110)	(112)	(113)
1	1	1	54.74°	35.26°	19.47°	29.50°
–1	1	1	125.26°	90.00°	61.87°	58.52°
1	–1	1	54.74°	90.00°	61.87°	58.52°
1	1	–1	54.74°	35.26°	90.00°	100.02°
–1	–1	1	125.26°	144.74°	90.00°	79.98°
1	–1	–1	54.74°	90.00°	118.13°	121.48°
–1	1	–1	125.26°	90.00°	118.13°	121.48°
–1	–1	–1	125.26°	144.74°	160.53°	150.50°

are given in Table 1. The (113) Si substrate was found to be suitable for the growth of semi-polar GaN(11–22) and GaN(20–21), because the angles between some Si(hkl) and planes and the surface (113) of the silicon substrate are close to the corresponding tilt angles.

To obtain GaN(10–11), the authors proposed a Si(100) substrate with disorientation at 7° at direction $\langle 110 \rangle$ (Fig. 8). The Si(100) substrate is subjected to a wet etching process using KOH solution (25 mass%) at 30°C [92] after pattern masking.

Since the bond energies of Si atoms are different depending on the crystal planes, and the Si(111) plane is inert to KOH, the process will automatically stop (Fig. 8, a). Then, one of the groove faces is coated with SiO₂, and the other face undergoes epitaxial growth in the direction perpendicular to the Si(111) face (Fig. 8, b).

Epitaxial growth of buffer layers of AlN with a thickness of 100–200 nm, followed by semi-polar GaN or AlN with a thickness of some μm was carried out by hydride vapor phase epitaxy in a hydrogen atmosphere on nanostructured NP–Si(100) substrates and, for comparison, on planar Si(111)-substrates. The epitaxy temperature of AlN was 1080°C, and GaN — 1050°C, the flow rates of HCl and NH₃ — 1.7 and 2.4 l/min, respectively.

Also, semi-polar GaN layers on NP–Si(100) substrates were grown by metalorganic vapour phase epitaxy on a modified EpiQuip setup with a horizontal reactor and an induction-heated graphite substrate holder. The structures consisted of an AlN layer with a thickness of ~ 20 nm and an unalloyed GaN layer with a thickness of $\sim 1 \mu\text{m}$. Ammonia (NH₃) and trimethyl gallium (TMG) were used as nitrogen and gallium sources, and hydrogen was used as the carrier gas — water. The reactor pressure during GaN growth was 100 mbar, and the substrate temperature was 1030°C.

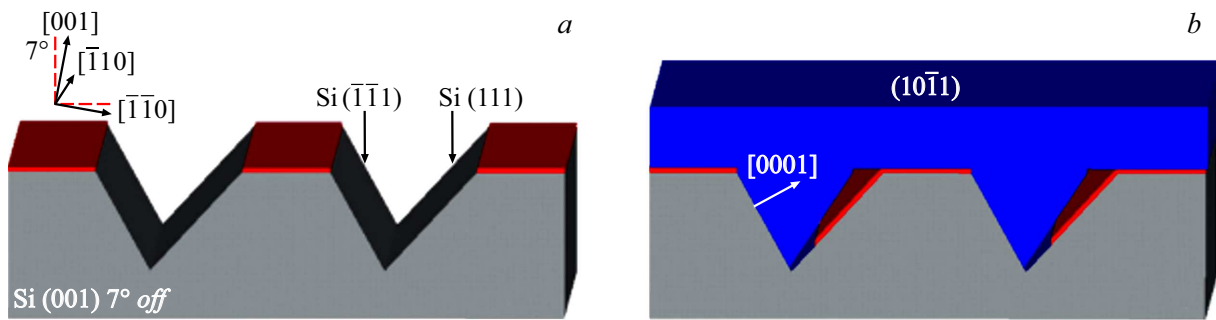


Figure 8. Schematic representation of Si(001) substrate after anisotropic KOH (a) etching. Schematic representation of GaN slope growth after fusion (b) [91].

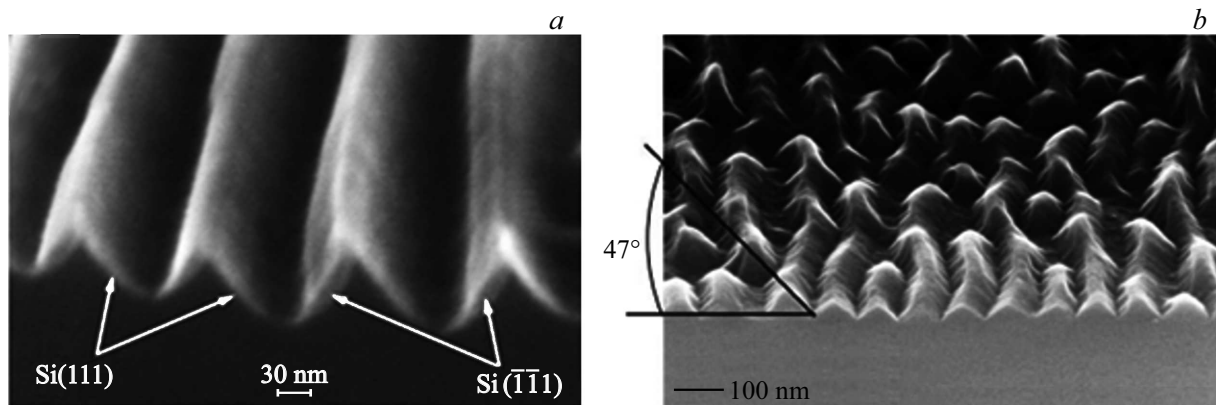


Figure 9. SEM images of the original NP–Si(100) nano-relief of substrates with different angles of Si(*hkl*): a — 54°, b — 47° [94].

1.2.1. AlN(10–11), AlN(10–12) on NP–Si(100)

1.2.1.1. Initial stages

This section is devoted to the study of the initial growth stages of semi-polar AlN grown by MOCVD on a nanostructured Si(100) substrate, on the surface of which V-shaped symmetric „ridges“ uncoated SiO₂ (NP–Si(100)) are formed. In experiments, we used structured NP–Si(100), substrates obtained by Wostec [93], which had V-shaped „nano-ridges“ with a period value between them of about 70 nm and a height of 30–50 nm (Fig. 9, a). Ridge angles were set by the parameters of the etching process. In experiment there were two types of substrates: the first, where ridges were etched at an angle $\approx 54^\circ$, targeting the singular Si(111)-plane, and the second type of substrates were etched at an angle $\approx 47^\circ$, targeting the deflected Si(111)-plane (Fig. 9, b). It should be noted, that the magnitude of the sloping Si(111) „facet of the nano-ridge“ was $l_{Si} \sim 75\text{--}90\text{ nm}$.

Chip images of structures with AlN layers synthesized on NP–Si(100)-substrate at an epitaxy temperature of $\sim 1080^\circ\text{C}$ in hydrogen flow showed that at thicknesses of about 15 nm, the AlN layer contains no crystals with visible faceting and follows the substrate surface (Fig. 10, a). At AlN thicknesses of about 30 nm, individual crystals faceted by planes (0001), (10–12), (10–11) are visible in the layer.

The faceting of AlN crystals was defined by planes (10–11) for blocks grown on ridge slopes with slope angle 54° (Fig. 10, b) and (10–12) for slope angle 47° .

The experiment showed that if the substrate has an inhomogeneous nanostructured surface, i.e., there are faces with an inclination angle to the Si(100) surface of both 47° , and 54° , then crystal quality will be low, and both AlN(10–12), and AlN(10–11) should be nucleated simultaneously. A similar pattern in the synthesis of gallium nitride on a structured sapphire substrate was observed by the authors [95].

In MOCVD modes, AlN growth is limited by the delivery of trimethyl-aluminium to the growing surface, and the AlN growth rate is proportional to the Al concentration in the reactor atmosphere minus the etch rate, which depends on temperature and hydrogen and ammonia concentrations. It is known that if the synthesis temperature of the AlN layer is high enough, the facets on the surface will appear as a plane (0001). If synthesis occurs below a certain temperature ($\sim 1390^\circ\text{C}$), other crystal planes such as (10–11) and (10–12) [96] may appear. When AlN is nucleated on a silicon substrate, a thin layer with no directional orientation is usually formed [97] (Fig. 10, a).

The main point of semi-polar layer formation is the process of crystal facet formation. As shown in Fig. 11, three-dimensional nanocrystals are formed on the slopes

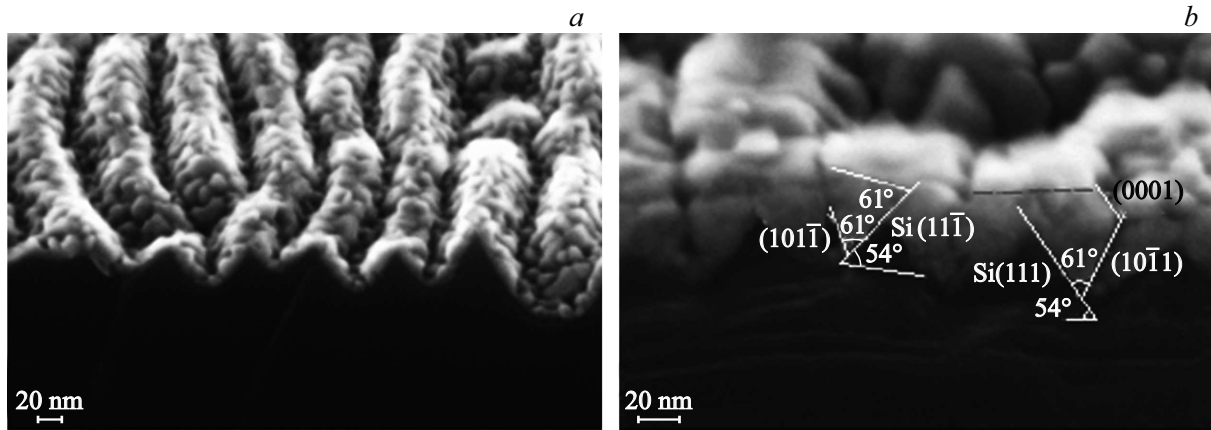


Figure 10. SEM image of the AlN chip and surface after synthesis at 0.5 (a) and 1 min (b) [98].

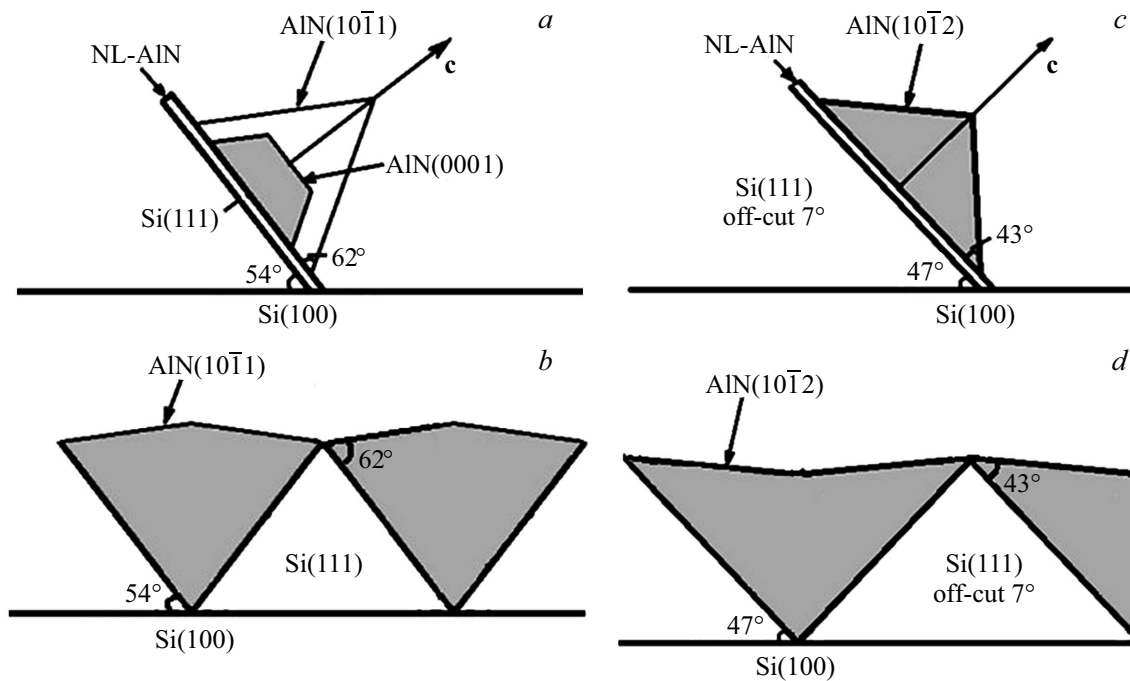


Figure 11. Schematic representation of AlN(10–11) (a, b) and AlN(10–12) (c, d) crystal formation on Si(100) [98] substrate

of the V-shaped structure, which grow in the direction of the axis c . Obviously, during the nucleation and initial growth stages of AlN, it is necessary to avoid subsequent nucleation, i.e. provide a density of AlN nucleation such that individual nuclei are separated by a characteristic distance l_{Si} , smaller than twice the Al-atom diffusion length distance L_{Al} . The diffusion path length of the Al adatom on the Si(111) surface is about $L_{Al} = 40$ nm [99]. In our case, $2L_{Al} > l_{Si}$, which means that we have a unique case, where the nucleation and growth of the AlN layer occurs under conditions of quasi-dimensional growth even at the epitaxy temperature not high for AlN $\sim 1080^\circ\text{C}$.

As is known [76], the angles between the plane AlN(0001) and AlN(10–11) — φ_1 or between

AlN(0001) and AlN(10–12) — φ_2 can be evaluated from the expression $\tan \varphi_1 = 2c/\sqrt{3}a$ and $\tan \varphi_2 = c/\sqrt{3}a$, where $c = 0.498$ nm, $a = 0.311$ nm. It is found that φ_1 and φ_2 are about 61 and 43°, respectively, which coincides with the crystal faceting planes (Fig. 11, a, b). The coalescence of the faceted crystals results in the formation of corrugated continuous layers of either AlN(10–11), or AlN(10–12) (Fig 11, c, d).

The observed differences in the faceting of AlN layer crystals during epitaxy on Si(111) faces with inclinations 54 or 47° to the Si(100) plane are related to the difference in the direction of the axis c , which, in turn, leads to different crystal planes of corrugated layers during nucleation on oriented or disoriented Si(111) faces of „nano-

ridge". Similar results were reported in [100], where the authors showed that substrate orientation and process conditions can control the growth of an isolated GaN block, leading to the formation of GaN structures with tilted axis c in various shapes. Epitaxy of GaN layers with thickness $\sim 1\ \mu\text{m}$ by MOCVD on AlN/NP–Si(100) templates yields GaN(10–12) or GaN(10–11) with X-ray diffraction curve half-width ω_θ with a value of 60 and 40 arcmin, respectively [101].

1.2.1.2. Raman light scattering

Raman light scattering spectra depend on both the crystal orientation and the concentration of charge carriers in the layer. Raman-active modes of light scattering are determined by the direction of incidence of the laser beam and the direction of polarization of the crystal, i.e. the Raman scattering selection rule. As it is known, in non-polar GaN crystals the light scattering modes with peaks $E_2(\text{high})$ and $A_1(\text{TO})$, $E_1(\text{TO})$ are active, while the peaks $E_2(\text{high})$ and $A_1(\text{LO})$ [102] appear for polar GaN crystals. Our results do not contradict this rule. The RS spectra of semi-polar AlN(10–12) show $E_2(\text{high})$ and $A_1(\text{TO})$ -, $E_1(\text{TO})$ -peaks, polar AlN(0001) — $E_2(\text{high})$, $E_1(\text{LO})$.

To compare the properties of the semi-polar and polar aluminium nitride layers, an AlN(0001) layer was additionally synthesized on a flat substrate in a similar temperature-time process. The epitaxial growth of layers was carried out by the HVPE method at the growth zone flux ratio $\text{H}_2:\text{NH}_3 = 2:1$ at a temperature of 1080°C . The thickness of the AlN layers was about $2\ \mu\text{m}$. X-ray diffraction analysis showed that the polar AlN(0001) layer synthesized on the planar Si(111) substrate has the half-width of the X-ray diffraction swing curve $\omega_\theta \sin 45$ arcmin, and the semi-polar AlN layer synthesized on the V-nanostructured substrate has a growth surface (10–12) with $\omega_\theta \sim 60$ arcmin.

The RS spectra of polar AlN(0001) and semi-polar (10–12)-layers (Fig. 12) contained lines belonging to the silicon substrate, peaks $E_2(\text{high})$ — $655.6\ \text{cm}^{-1}$, which are the same for both structures, with almost identical half-widths of $E_2(\text{high})$ peaks. The RS spectra of polar and semi-polar AlN layers have significant differences: the polar layer contained a peak of 887.5 , which is attributed to $A_1(\text{LO})$ phonon [103], while the semi-polar — peaks of 668.1 and $907.3\ \text{cm}^{-1}$, attributed to $E_1(\text{TO})$ $E_1(\text{LO})$ -phonons. $A_1(\text{TO})$ peaks differed both in the position of the maxima (607 and $617\ \text{cm}^{-1}$ for polar and semi-polar layers, respectively) and in intensity (the semi-polar has higher intensity) (Fig. 12).

The broadening of the RS spectra is usually the result of phonon scattering, caused by small block layer grains, by a stress gradient in the heterostructure. For bulk AlN crystals, the FWHM of the $E_2(\text{high})$ peak has a value of $3\text{--}5\ \text{cm}^{-1}$ [103], and for a polycrystalline layer it can be as large as $50\ \text{cm}^{-1}$ [105]. The enhancement of the A_1 peak (TO) and the appearance of the $E_1(\text{TO})$ in the semi-polar

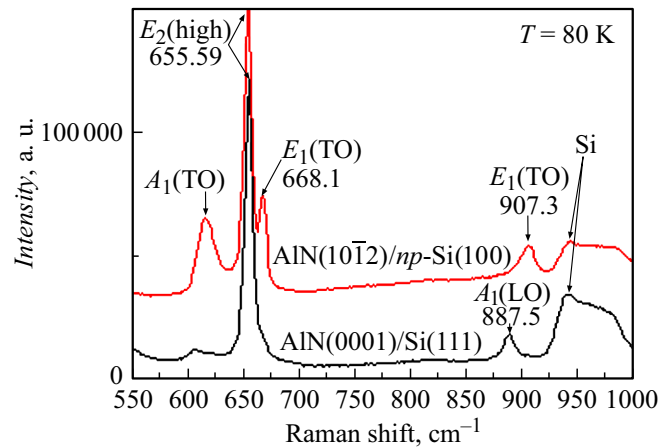


Figure 12. RS spectra of AlN(10–12)/NP–Si(100) and AlN(0001)/NP–Si(111) [104].

structure compared to the polar structure can be interpreted as follows.

1.2.2. AlN(10–11)/NP–Si(100): plastic relaxation

We consider the conditions of occurrence and results of plastic relaxation of a stressed semi-polar AlN layer with a thickness of about $7\ \mu\text{m}$ grown by the HVPE method on an NP–Si(100) [106] substrate.

SEM images revealed that, first, the V-structured surface is preserved during HVPE synthesis, second, at this thickness, the AlN(10–11) layer contains a grid of parallel quasi-periodic cracks that stretch along the growth direction and are strictly perpendicular to the NP–Si(100) ridges with a spacing of about $135\ \text{nm}$ (Fig. 13, *a*), and, thirdly, the crack penetrates not only the AlN layer with thickness $7\ \mu\text{m}$, but also partially penetrates the Si substrate to a depth of $300\ \text{nm}$ (Fig. 13, *b*). A similar system of parallel cracks was observed in the synthesis of semi-polar GaN(20–23) layers (Fig. 6) by HVPE method on a disoriented Si(100) substrate.

To explain the cracking conditions in the semi-polar AlN layer synthesized on NP–Si(100)-substrate, we first estimate the magnitude of the tensile stress in the AlN(10–11)-layer at which cracks occur (σ_{cr}), and compare it with the magnitude of the elastic stresses that occur during cooling of the AlN structure on the Si substrate. It is known that the energy Γ , at which crack formation occurs in AlN, is a value of $4.81\ \text{J/m}^2$ [107]. The experimentally determined crack spacing AlN/NP–Si(100) is $L = 135\ \text{nm}$ (Fig. 14), then, according to [108], we can determine the critical stress at which crack formation occurs in AlN/Si structure

$$\sigma_{\text{cr}} = \sqrt{5.8 \frac{\Gamma E_{\text{AlN}}}{L(1 - \nu_{\text{AlN}}^2)}}, \quad (1)$$

where $E_{\text{AlN}} = 225\ \text{GPa}$ for AlN/Si [109] and $\nu_{\text{AlN}} = 0.24$ — the Young's modulus and Poisson's ratio, respectively.

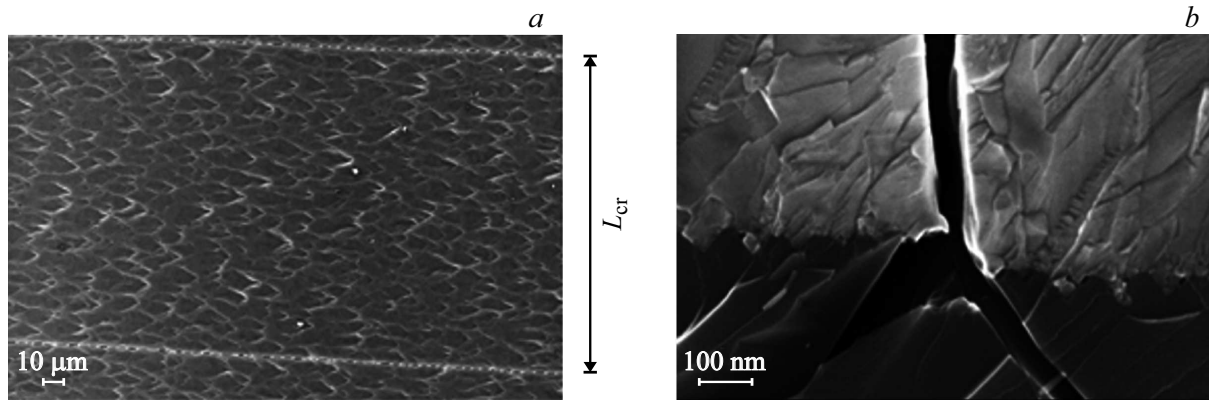


Figure 13. SEM image: *a* — surface of semi-polar AlN(10–11) with quasi-periodic cracks, *b* — slice of AlN/NP–Si(100) structure with crack [106].

It is found that the critical stress value in the AlN(10–11), layer, at which cracks occur is 0.22 GPa. We compare this value with the elastic stresses σ_f , which can occur in an AlN layer when the structure is cooled from the epitaxy temperature T_1 — 1080°C to room temperature T_2 — 25°C by formula [110]:

$$\sigma_f = \frac{E_{\text{AlN}}}{1 - \nu_{\text{AlN}}} \frac{(\alpha_{\text{AlN}} - \alpha_{\text{Si}})(T_1 - T_2)}{1 + \frac{E_{\text{AlN}}(1 - \nu_{\text{Si}})h_{\text{AlN}}}{E_{\text{Si}}(1 - \nu_{\text{AlN}})h_{\text{Si}}}}, \quad (2)$$

where $h_{\text{Si}} = 400 \mu\text{m}$, $h_{\text{AlN}} = 7.5 \mu\text{m}$ — thicknesses of the Si substrate and AlN layer, respectively, $\alpha_{\text{Si}} = 3.6 \cdot 10^{-6} \text{ K}^{-1}$, $\alpha_{\text{AlN}} = 5.3 \cdot 10^{-6} \text{ K}^{-1}$ [111] — the coefficients of thermal expansion of the substrate and layer, respectively, $E_{\text{Si}} = 131 \text{ GPa}$ for Si(111) and $\nu_{\text{Si}} = 0.26$ — the Young’s modulus and Poisson’s ratio, respectively.

It turned out that the value of $\sigma_f = 0.5 \text{ GPa}$ is significantly higher σ_{cr} . The formation of cracks in AlN and Si (Fig. 13, *b*) apparently occurred as a result of abrupt plastic relaxation during cooling, which is confirmed by the type of cracks.

In the HVPE method, the growth of the semi-polar AlN layer occurs perpendicular to the Si(111) plane. The size of the AlN block in the growth direction is smaller than the threshold distance $L_{\text{cr}} = 135 \text{ nm}$, so no cracks occur in this direction (Fig. 14). In the direction along the ridge, the size of the layer is larger than L_{cr} , in which case, the elastic stress will exceed the threshold value and a system of quasi-cracks will appear (Fig. 14).

An anisotropic model for stresses in gallium nitride and aluminium nitride films grown on Si(111) substrates caused by thermal mismatch between film and substrate is published in [63]. The authors determined the stresses in the layers by Raman light scattering spectral curve frequency shifts and observed good agreement with the model for polar III-nitride layers. In paper [112], the mechanisms of mismatch stress relaxation in heterostructures of LED based on semi-polar GaN have been analyzed within the energy approach taking into account crystallographic features and

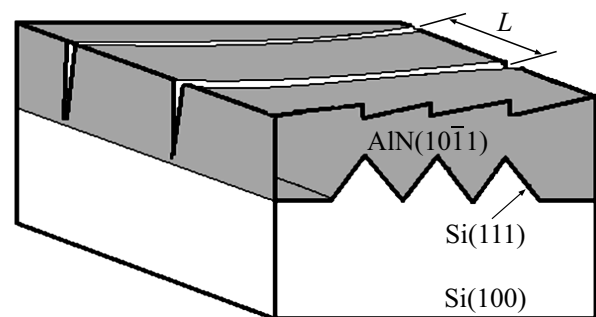


Figure 14. Schematic representation of cracks in the AlN/NP–Si(100) [106] structure

elastic anisotropy of the crystal lattice of wurtzite III-nitride. Calculations have shown that the value of the angle between the polar c axis in the wurtzite structure and the growth direction of the heterostructure is essential for predicting different mechanisms of mismatch stress relaxation.

1.2.3. GaN(10–11)/NP–Si(100): self-forming mask model

In paper [113], the growth of GaN on Si(001) substrates with micron-sized V-groove by MOCVD and the photoluminescence of semi-polar{1–101}InGaN/GaN structures were studied. Photoluminescence measurements at different intensities have shown that the internal electric field in a multi-quantum InGaN/GaN MQW structure grown on a semi-polar GaN(1–101), layer is indeed smaller than that of an MQW structure grown on polar GaN(0001), but the mechanism of semi-polar layer formation for the V-shaped structure is not represented in the literature.

In this section, we discuss the features of the transition from the symmetric state of two semi-polar planes with oppositely oriented c -axes to the asymmetric state with a single c -axis orientation of III-nitride layers during synthesis on V-shaped symmetric nanostructured silicon substrates

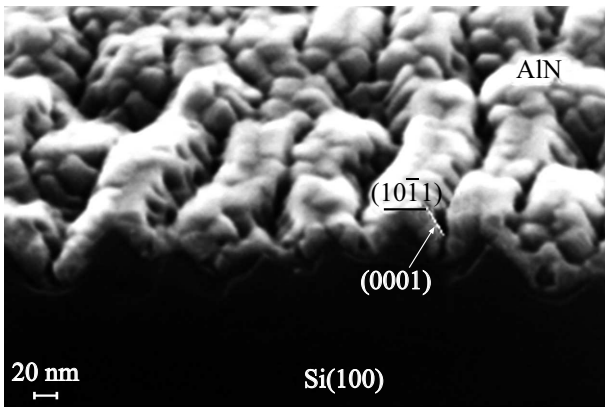


Figure 15. SEM image of AlN/NP–Si(100)-structures at the initial growth stage

and the development of a model that relates this transition to the formation of the substrate nano-mask.

Scanning electron microscope images of the spall and the AlN surface show that the layer forms a corrugated surface consisting of two semi-polar AlN(10–11) with opposite c -axes. When the average thickness of the AlN layer on the slopes of the nano-ridge is about 35 nm (Fig. 15), it can

be seen that the chipped samples do not show any sign of structure asymmetry.

The spall image showed that after GaN synthesis, the nanostructured AlN is preserved (Fig. 16, *a*), but there is a transition from the symmetric state of two semi-polar planes of AlN(10–11) with opposite c -axes to the asymmetric state of GaN(10–11) (Fig. 16, *b*) with a single orientation of the c -axis, and its direction coincides with the direction of the flow of N_2 ions onto the silicon surface during the formation of nano-masks (Fig. 16).

In this regard, to search for the reasons for the above transition from the symmetric state to the asymmetric state, one should turn to the WOS-nano-mask as the basis for the formation of NP –Si(100). The nano-mask is formed through a two-step process. In the first stage, upon bombardment with an inclined flux of N_2^+ nitrogen ions, the collision cascade areas merge into a continuous anisotropically stressed modified layer. In second stage, the increase in wave amplitude is caused by ion sputtering without changing the period of the structure. As a result, ion-synthesized silicon nitride nano-bands are formed on the wave slopes facing the ion flow, with the SiN nano-bands exhibiting strong compressive stresses (Fig. 17, *a*). Accordingly, the near-surface silicon layer appears anisotropically periodically stressed to a sufficient depth of several WOS wavelengths and has tensile stresses

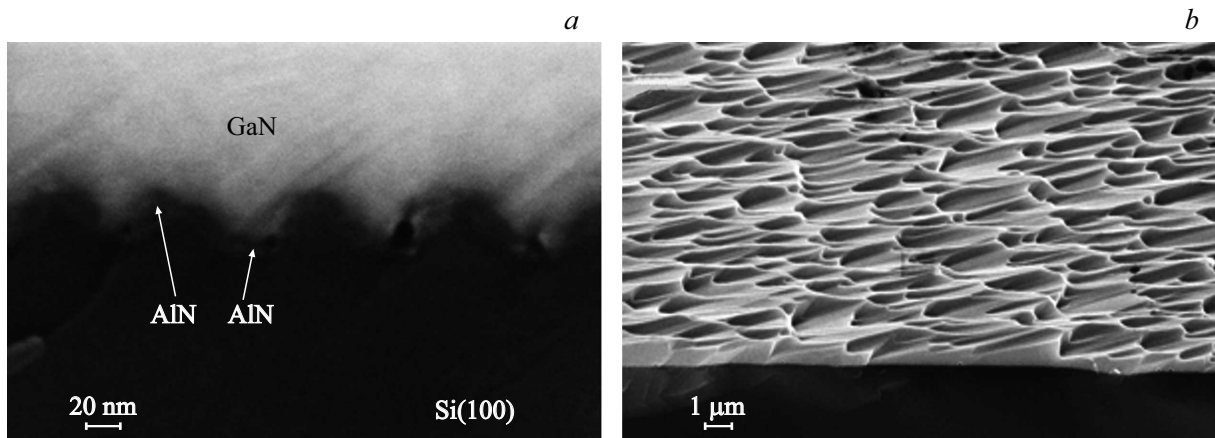


Figure 16. SEM image of the chipped (*a*) and surface (*b*) GaN(10–11)/AlN/NP–Si(100)-structure [98].

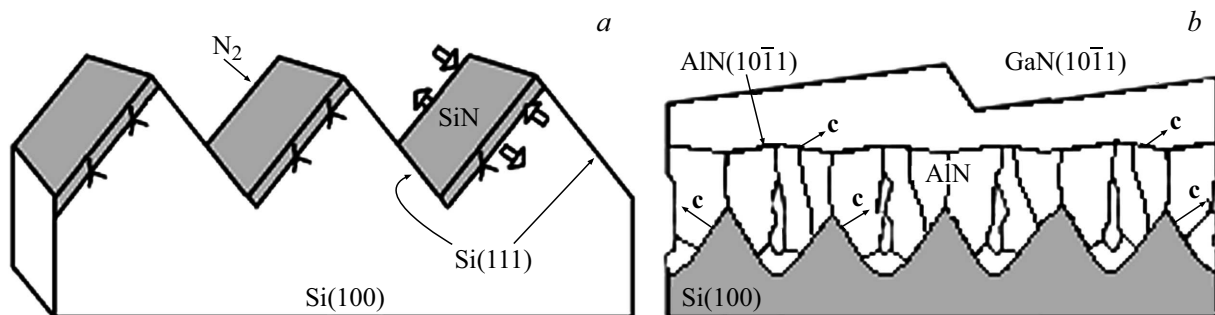


Figure 17. Schematic representation of stresses due to WOS nano-mask and ion flow direction N_2^+ (*a*) and epitaxial growth of corrugated AlN(10–11)- and GaN(10–11)-layers with a single orientation of c -axis (*b*) [98].

(Fig. 17, *a*). Defects are formed in the stressed near-surface layer of silicon, similar to what was observed in [114].

Stresses and defects during etching in KOH and after SiN removal are not visually apparent, and geometrically symmetrical faces (111) and $(-1-11)$ (Fig. 9, *a*), are formed in V-shaped nano-ridges, where defects are present only on the slopes of nano-ridges $(-1-11)$, and the other slope (111) remains practically free of defects.

The epitaxy of the AlN layer forms a corrugated AlN(10–11), surface on facets with different strain values of the growing layers, and these two facets of the surface have different numbers of defects because they are synthesized on silicon facets with different degrees of defects. The more defective plane of the corrugated layer should have a higher growth rate compared to the growth rate of the competing plane and accordingly the GaN epitaxy process exhibits a faster growing plane on the surface — GaN(10–11) [98].

Thus, the experimentally detected effect of transition from the symmetric state of semi-polar linear nano-crystallites AlN(10–11) with opposite *c*-axes, which are formed on symmetric silicon nano-ridges NP–Si(100)-substrate, to the asymmetric state with a single orientation *c*-axis of GaN(10–11)-layer, according to the self-forming mask model, may be due to the properties of the WOS process.

1.2.4. GaN(10–11)/NP–Si(100):surface energy model

The formation of semi-polar III-nitride layers on NP–Si(100)-substrate with a single *c*-axis orientation may be based on differences in the formation of AlN(10–11) layers on the Si(111) face and AlN(10–1–1) layers on the Si $(-1-11)$ face due to different surface energy. The values of surface energies known in the literature are rather averaged, and the influence of surface structuring is not taken into account. Thus, the calculated surface energy of ideal AlN and GaN surfaces with polar and semi-polar orientations according to [115] shows that polar planes have smaller values than semi-polar planes (1–101) and (11–22) (Table 2).

The data on the surface energy of ideal GaN surfaces with polar and semi-polar orientations under conditions of a gas atmosphere enriched with nitrogen atoms show that the energy values also depend on the orientation of the fac [116].

It can be seen that the energy increases depending on the orientation of the GaN surface in the following

Table 2. surface energy of ideal AlN and GaN (eV/A²) surfaces with polar and semi-polar orientations [99]

surface	(0001)	(000–1)	(1–101)	(11–22)	(11–20)
AlN	0.250	0.255	0.261	0.259	0.170
GaN	0.185	0.228	0.193	0.194	0.141

Table 3. surface energy of GaN surface facets in an atmosphere enriched with nitrogen atoms [116]

Surface	(0001)	(000–1)	(1–101)	(1–10–1)	(11–22)	(11–2–2)
eV/A ²	0.204	0.234	0.224	0.257	0.221	0.250

order: (0001), (11–22), (1–101), (000–1), (11–2–2) and (1–10–1). The corrugated AlN surface leads to the synthesis of GaN(1–101) and GaN(1–10–1) [8], layers, which have different surface energies (Table 3). These differences can provide different growth rates of GaN facets and lead to the formation of GaN layer in one direction (Fig. 16, *b*, 17, *b*).

The detected effect of transition from the symmetric state of semi-polar linear nano-crystallites AlN(10–11) with opposite *c*-axes, which are formed on symmetric silicon nano-ridges NP–Si(100)-substrate, to the asymmetric state with a single orientation *c*-axis of GaN(10–11)-layer, according to the model, can be determined by the difference in the surface energy of the (10–11) and (10–1–1) facets of AlN and GaN layers.

1.2.5. GaN(10–11)/AlN/3C–SiC/NP–Si(100)

1.2.5.1. Growth features

Consider the synthesis of semi-polar gallium nitride layers grown on an NP–Si(100) substrate using a pre-formed 3C–SiC thin layer on its surface. The NP–Si(100) substrates were V-shaped grooves, on whose surface SiC [80] nanocrystals were synthesized by solid-phase epitaxy technology. GaN layers on the substrates were grown by MOCVD in a hydrogen atmosphere. The structures consisted of an AlN layer with a thickness of ~ 20 nm and an unalloyed GaN layer with a thickness of ~ 1 μ m. Three types of GaN layers synthesized on flat Si(100) substrate, on NP–Si(100) substrate and on SiC/NP–Si(100) template were investigated.

X-ray diffraction and SEM analyses of GaN layers synthesized in the same process on flat Si(100) substrate, on NP–Si(100) substrates and SiC/NP–Si(100), templates showed different crystallographic surface structure of GaN layers (Fig. 18, *a, c, e*). On flat Si(100)-layer substrate was synthesized in the GaN(0001) direction (Fig. 18, *a, b*) with the half-width of the GaN(0002) X-ray diffraction curve ω_θ about 120 arcmin, and on the NP–Si(100) and SiC/NP–Si(100) — in the semi-polar GaN(10–11) direction with $\omega_\theta \sim 60-45$ arcmin (Fig. 18, *c, d, e, f*) respectively. We pose that the presence of different surface energy values of AlN(10–11) on the Si(111) face and AlN(10–1–1) on the Si $(-1-11)$ face with an intermediate thin 3C–SiC-layer will lead to different GaN rates on these faces and synthesis in the same semi-polar direction (Fig. 19).

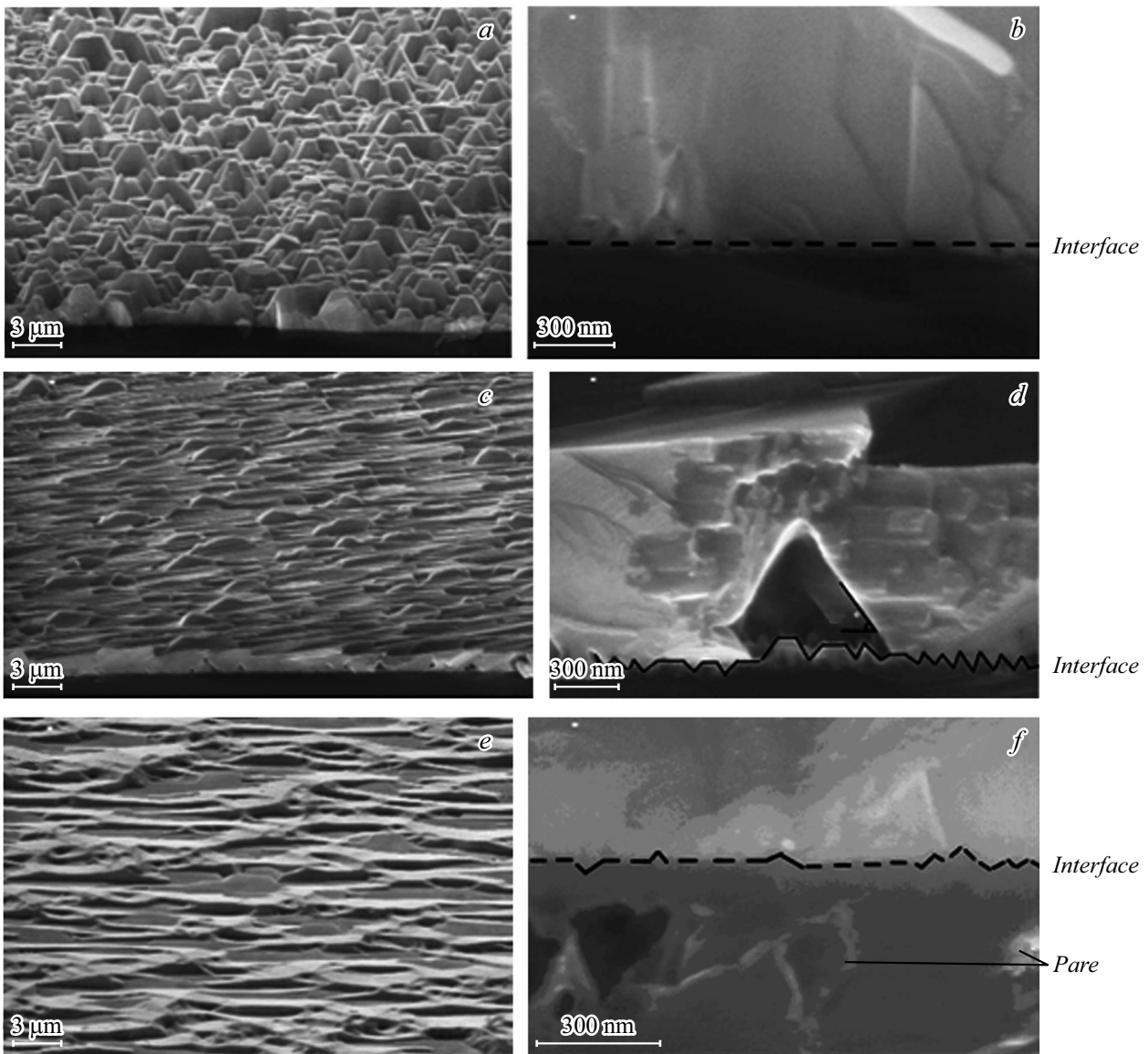


Figure 18. SEM images and spalling of GaN(0002)/Si(100) (a, b), GaN(10–11)/NP–Si(100) (c, d) and GaN(10–11)/SiC/NP–Si(100) (e, f) [117].

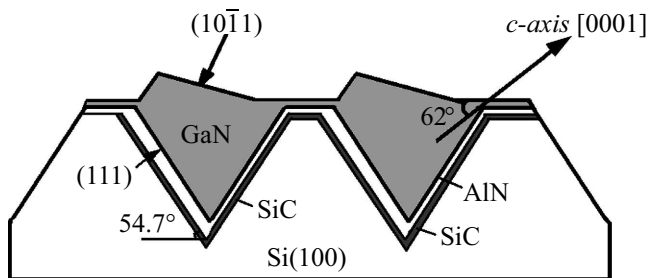


Figure 19. Schematic of GaN(10–11) formation on NP–Si(100) [117] surface.

The semi-polar GaN(10–11), layers synthesized on SiC/NP–Si(100)-substrate had less rough surface than those synthesized on NP–Si(100) without SiC-layer. AFM images

of the GaN/AlN/SiC/NP–Si(100)-structure showed that the surface had a pronounced asymmetric pattern, with a base roughness of about 250 nm and GaN(10–11) protrusions of about 500 nm were present

So, hetero-epitaxy of GaN layer on V-shaped nanostructured NP–Si(100), substrate, combined with synthesis of nanoscale SiC layer formed by solid-phase replacement of silicon atoms with carbon atoms, leads to the growth of GaN(10–11) layer due to the competitive process of formation of AlN and GaN layers on the walls of nanochannels.

1.2.5.2. Photoluminescence

The photoluminescence spectra of GaN(10–11), GaN(10–12), synthesized on NP–Si(100) and

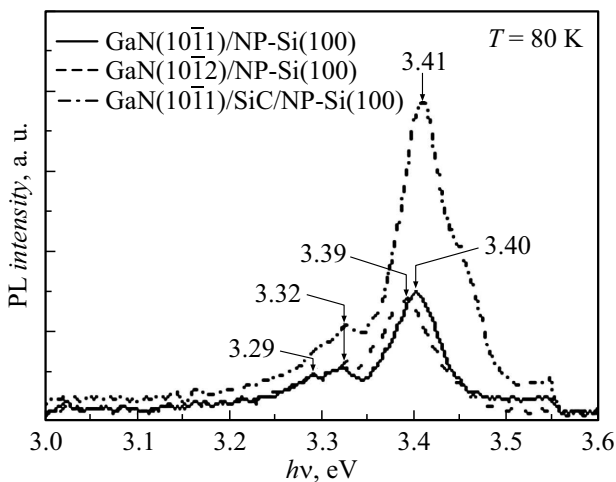


Figure 20. Photoluminescence spectra of GaN(10–11)/NP–Si(100), GaN(10–11)/SiC/NP–Si(100) and GaN(10–12)/NP–Si(100) [121] structures.

GaN(10–11) on SiC/NP–Si(100), are different. Thus, the energies of the maximum spectra of GaN(10–11)/NP–Si(100) — $h\nu_1 = 3.40$ eV, $h\nu_2 = 3.32$ eV, $h\nu_3 = 3.29$ eV, GaN(10–11)/SiC/NP–Si(100) — $h\nu_1 = 3.39$ eV and GaN(10–12)/NP–Si(100) — $h\nu_1 = 3.41$ eV (Fig. 20).

In the luminescence spectra of semi-polar crystals, the $h\nu$ 3.40–3.41 eV, line associated with packing faults — BSF_S I₁ (basal plane stacking faults) [118], which occurs during nucleation by the Volmer–Weber [119] mechanism, is usually observed.

The model of luminescence due to stacking faults is first proposed in [120] and suggests that excitons in GaN can bind to stacking faults as in an ideal quantum well of cubic GaN surrounded by wurtzite GaN.

By analogy with the photoluminescence data [122], we can conclude that the $h\nu = 3.39$ –3.40 eV peak in GaN(10–11) layers and the $h\nu = 3.41$ eV in GaN(10–12) are due to BSF_S I₁ defects. The $h\nu = 3.30$ –3.32 eV peak is possibly due to donor-acceptor recombination associated with silicon in GaN atoms.

So, the luminescent properties of the semi-polar layers are due to stacking faults — BSF_S–I₁.

1.2.6. GaN(11–22)/NP–Si(113)

1.2.6.1. Initial growth stages

Let us consider the initial stages of GaN(11–22) layer formation on a nanostructured Si(113) substrate (Fig. 21).

The substrates NP–Si(113) were formed using the technology outlined previously. The structures were synthesized by MOCVD and consisted of an AlN layer with a thickness of ~ 20 nm and two types of GaN layers with different thicknesses: an island GaN layer with dimensions ~ 0.05–0.1 μm and a continuous GaN(11–22) layer with a thickness of 0.5–1 μm. X-ray diffraction analysis of the

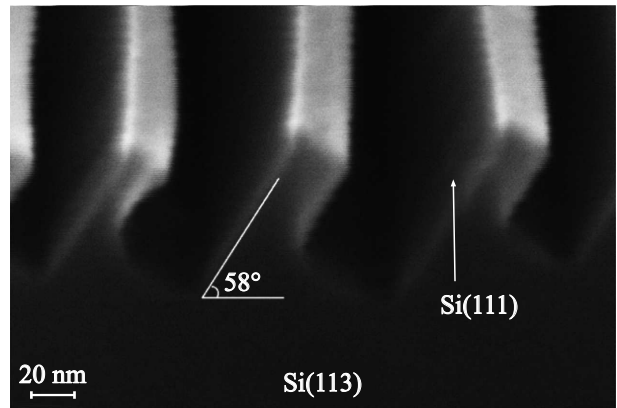


Figure 21. SEM image of a chipped NP of –Si(113) substrate.

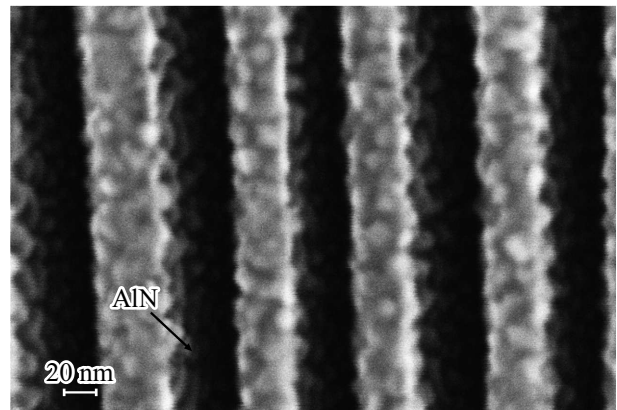


Figure 22. SEM is an image of the surface NP–Si(113) of a substrate coated with a thin layer AlN [123].

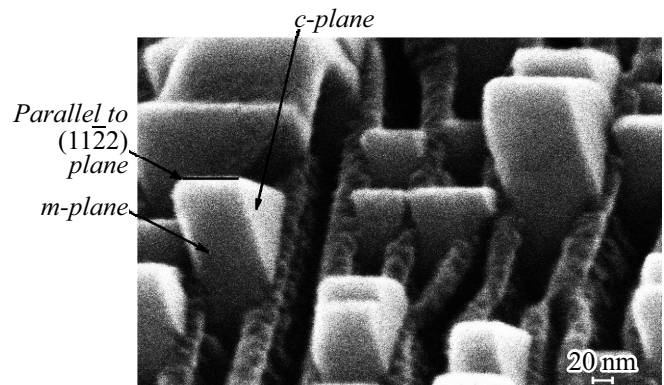


Figure 23. SEM is an image of the GaN insular layer at the initial stage of growth [123].

layers showed that the solid layers of GaN(11–22) have a half-width of the X-ray diffraction curve $\omega_{\theta} \sim 30$ arcmin.

The scanning-electron microscope image of the surface showed that on the NP–Si(113) nanostructured substrate, the AlN layer uniformly covers the surface (Fig. 22), and nucleation of GaN occurs on the surface of the AlN/Si(111) facet by island mechanism (Fig. 23), and

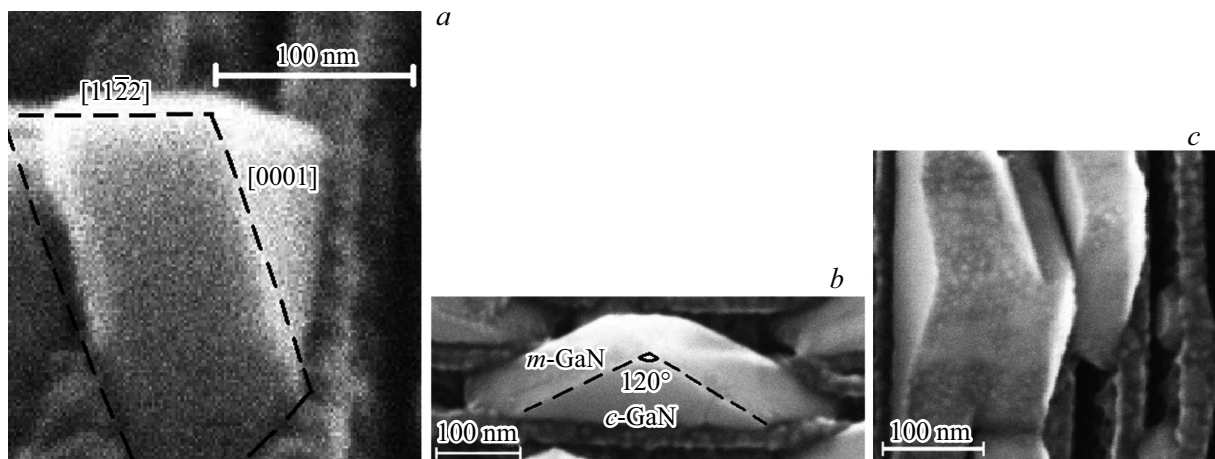


Figure 24. SEM image of the facets of the GaN island; *a* — *m*-GaN, where the dashed lines show the edges [11–22] and [0001], *b* — GaN(0001), *c* — the top view of *m*-GaN and *c*-GaN [123].

the shape of the island (Fig. 24) shows the presence of GaN(0001), *m*-GaN planes. The average thickness of the islands in the direction perpendicular to the groove was 100 nm (Fig. 24, *a*), and in the direction along the groove about 160 nm (Fig. 24). It can be seen that the crystals are faceted in the direction along the groove, in our opinion — *m*-GaN with an angle of 120° between the facets and GaN(0001) in the perpendicular to the Si(111) plane (Fig. 24). An *m*-GaN face has a rectangular shape, with an edge that belongs to two neighboring planes of *m*-GaN lying parallel to the plane (11–22). It can be seen that the selective growth of GaN(11–22) on NP–Si(113) is accompanied by the formation of voids (voids) in the area of the bottom of the nanochannels, which should provide stress relaxation in the layer GaN [122].

The larger size of the nucleus (Fig. 24, *c*) in the direction along the „of the nanochannels“ than in the direction perpendicular to them can be explained by the different path length of Ga (*L*) adatoms during the formation of the island layer. It is known that, $L = (Dt)^{1/2}$, where *D* — the diffusion constant of Ga atoms on the surface, and *t* — the lifetime of Ga adatom on the surface of the nanostructure. The constant *D* depends on the epitaxy temperature, which was constant throughout the growth, and we assume that *D* is the same in both directions and hence there remains an influencing factor *t*. When atoms diffuse along the „of the“ nanowires, the adatoms on the surface have a larger magnitude *t*, than in the direction perpendicular to the „nanowires“. This is probably due to the presence of „nanohills“ in the direction perpendicular to the „nano-canaries“ which lead to impaired surface diffusion and reduced *t*, and hence a shorter waviness period and smaller island size in this direction (Fig. 24, *c*).

Note that the observed faceting of a GaN crystal during synthesis on a silicon substrate occurs as a result of nonequilibrium processes, which are influenced by the values of supersaturation of gallium atoms, crystal deformation during GaN/Si heteroepitaxy, as well as, the difference in the length

of the diffusion path of Ga atoms in the directions along and across the groove.

As is known, the faces of GaN embryo should be formed in accordance with the Gibbs-Curie-Wolfe principles—, which require the formation of a crystal with the lowest surface free energy. The facet of a crystal growing under equilibrium conditions is formed by facets with minimum values of specific surface energy [124]. Note, that crystals with covalent, ionic, or metallic bonds strongly stick together when they collide, making it difficult to form faces [125]. Usually, when a crystal grows, its faces move in a direction perpendicular to their planes, and the higher the growth rate, the greater the specific surface energy of the face.

As can be seen from the table, the specific surface energy GaN(0001) — 0.185 eV/A² and GaN(10–10) — 0.141 eV/A² imply that the growth rate of the *c*-GaN face should be greater than *m*-GaN, and consequently, the layer thickness in the direction of GaN(0001) should be greater than in the direction of *m*-GaN. However, this is not confirmed in the experiment. We believe that this behavior of the growth rate of the face GaN(0001) is due, perhaps, firstly, to the effect of the deformation of the face (0001) during epitaxy on the wall of the groove Si(111), which should reduce the value of the specific surface energy GaN(0001), and secondly, the differences in the diffusion length of Ga atoms along and across the groove. The change in the value of the surface energy GaN(0001) under the impact of elastic stresses of the surface was noted in [126].

The appearance of the crystal configuration when the edge is parallel (11–22) can be explained by the growth features of gas-phase epitaxy. All growth parameters can be represented by one thermodynamic epitaxy parameter — supersaturation of vapors Ga — γ_{Ga} , which measures the deviation of the system from equilibrium and represents the driving force for the formation of GaN and depends on the

partial pressure Ga in the gas medium [127]

$$\gamma_f = (P_{in}^{Ga} - P_{eq}^{Ga})/P_{eq}^{Ga},$$

where P_{in}^{Ga} is the input partial pressure, and P_{eq}^{Ga} is the equilibrium vapor pressure Ga at the interface of the vapor–solid body.

In turn, the chemical potential of gallium μ_{Ga} is associated with the oversaturation of Ga [128] atoms as

$$\mu_{Ga} \sim kT \log(1 + \gamma_{Ga}).$$

For example, calculations performed in [129] for three surfaces for μ_{Ga} , showed that semi-polar faces (11–22) are formed at high supersaturation of Ga vapors, while nonpolar(11–20) faces are preferable at low supersaturation of Ga vapors.

The surface differences of the semi-polar face from the polar and nonpolar ones lead both to a difference in the specific surface energy of the faces and to the crystallographic dependence of the face on the supersaturation of Ga atoms in the gas composition.

Since the surface energy of the semi-polar facet of GaN(11–22) is larger than that of the non-polar GaN(10–10), only non-polar or polar facets should remain at high growth temperature ($T = 1030^\circ\text{C}$) under conditions where the μ_{Ga} supersaturation value is large.

The authors [130,131] have shown that synthesis of GaN(11–22) on a Si(113) substrate structured as formed periodic square windows completely eliminates one of the most important problems in growing semi-polar GaN on silicon substrates — „reverse melting Ga“. In result, crack-free semi-polar GaN(11–22) was obtained with significant improvements in crystal quality, in particular, stacking defects BSFs were reduced.

The authors [132,133] have shown that a two-step approach has been developed to grow semi-polar (11–22) GaN on structured Si(113) substrates, which effectively eliminates etching of the Ga melt at high temperature. A grooved structure was deposited on a (113)Si substrate by using a standard micron-scale photolithography technique, then anisotropic chemical etching was used to form a Si(111) face and then a thick layer of AlN was epitaxially grown on the structured silicon to cover all the faces and ensure that no Ga atoms were in contact with the substrate. In further, we applied the SiO₂ mask only on (113) facets to ensure that GaN grew only on the exposed (111) facets, and thus formed (11–22) semi-polar GaN with high crystal quality along the vertical direction. Low-temperature photoluminescence measurements confirm a significant reduction in the density of basal stacking defects (BSFs).

Si(112) and Si(115) substrates were used for epitaxial growth of nitride multilayer structures. It was found, that substrate orientation and process conditions can control the growth of an isolated GaN block, leading to the formation of GaN structures with tilted axis *c* in different directions [100].

We report [134] growth of semi-polar (20–21) GaN layers on a structured Si(114) substrate by MOCVD. The

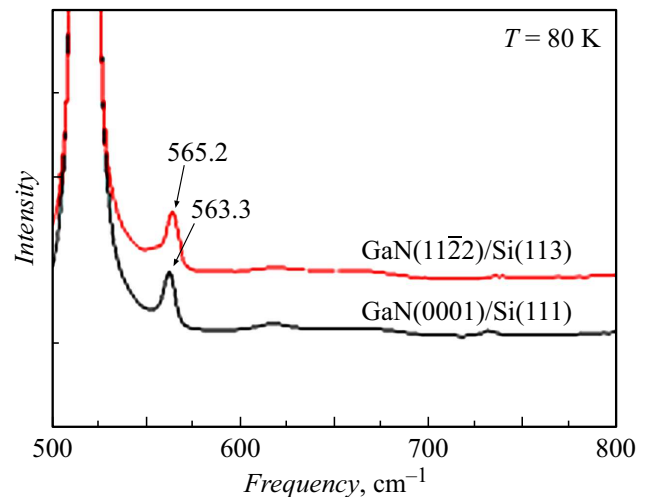


Figure 25. Raman scattering spectra of GaN(11–22)/Si(113) and GaN(0001)/Si(111) [104].

fusion of neighboring blocks with GaN nucleated on the exposed Si(111) faces leads to the formation of a continuous GaN(20–21)-layer, which has a faceted morphology. X-ray rocking curve measurements showed that the FWHM values are 610 and 1490 arcsec when measured in the direction perpendicular and parallel to the striations of the structured surface, respectively.

The growth of GaN(20–21)-layers on a structured Si(113) substrate has also been demonstrated in [135]. X-ray rocking curves of GaN(20–21) on Si(113) substrate at FWHM values of 535 and 504 arcsec were obtained by scanning along the GaN [0001] and [11–00] directions, respectively.

1.2.6.2. Raman scattering

We consider the deformation of semi-polar GaN(11–22) layers during epitaxy on an NP–Si(113) substrate. Two samples — semi-polar layers GaN(11–22) on NP–Si(113) and, for comparison, polar GaN(0001) on a flat Si(111) substrate were grown by MOCVD in the same temperature and time regimes. The structures consisted of an AlN layer with a thickness of 20–30 nm and an unalloyed GaN layer with a thickness of $\sim 1\ \mu\text{m}$. X-ray diffraction analysis of the layers showed that the layers have an X-ray diffraction curve half-width of $\omega_\theta \sim 30$ arcmin for GaN(11–22) and ~ 22 arcmin for GaN(0002).

Investigation of GaN(11–22)/ NP–Si(113) and GaN(0001)/Si(111) heterostructures by RS revealed a difference in the deformation of the structures during epitaxy on a flat Si(111) substrate and on a templated NP–Si(113). The RS spectra measured in the $E_2(\text{high})$, phonon mode area for GaN layers grown on NP–Si(113) and Si(111), were generally in line with what would be expected, containing lines belonging to the silicon substrate and $E_2(\text{high})$, lines due to gallium nitride. The position

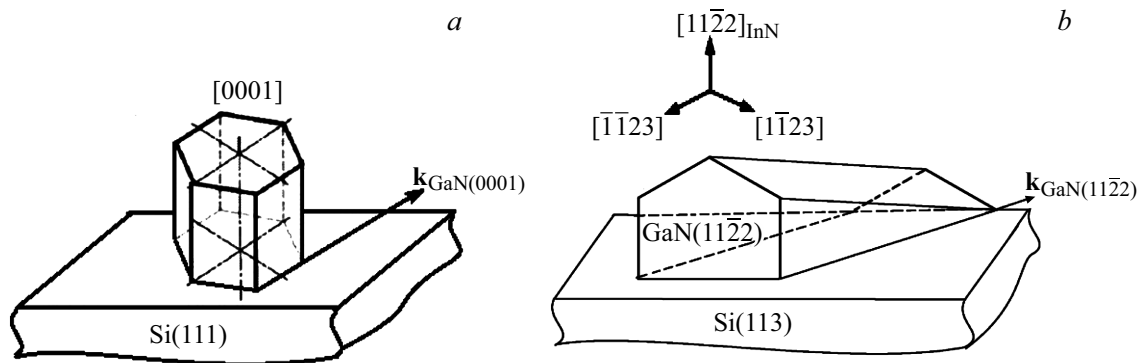


Figure 26. Schematic representation of the ratios of the thermal expansion coefficients of GaN(0001) (a) and GaN(11–22) (b) layers on silicon [104] substrates

of the $E_2(\text{high})$ line depended on the structure and was 563.3 cm^{-1} for GaN(0001)/Si(111) and 565.2 cm^{-1} for GaN(11–22)/NP–Si(113) (Fig. 25).

The difference in the position of the $E_2(\text{high})$ lines for these structures can be explained as follows. It can be clearly seen from the RS data that the position of the $E_2(\text{high})$ line peak for GaN layers is shifted to the low-frequency side with respect to its position in the non-deformed layer (it was assumed that for the unstressed structure the position of $E_2(\text{high}) = 568 \text{ cm}^{-1}$), which indicates the presence of GaN stretching strain in the plane parallel to the substrate plane. For GaN(0001) and GaN(11–22) layers, the magnitude of longitudinal elastic stresses — σ was evaluated. The values of σ were found to vary considerably: $\sigma_{(0001)} = 1.12 \text{ GPa}$ and $\sigma_{(11-22)} = 0.67 \text{ GPa}$ respectively, for GaN(0001)/Si(111)- and GaN(11–22)/NP–Si(113)-structures.

The elastic stress values obtained include residual elastic stresses $\sigma_{\Delta\alpha}$, which occur at epitaxy temperature $\text{GaN} = 1030^\circ\text{C}$, and stresses $\sigma_{\Delta\alpha}$, which occur during cooling of GaN(0001)/Si(111) and GaN(11–22)/NP–Si(113) structures. Since the nucleation and growth of the GaN layer occurs on the Si(111) plane or on Si(111) faces, we assume that the residual elastic stresses at epitaxy temperature $\sigma_{\Delta\alpha}$ will be the same for both types of structures, while the stresses that arise on cooling may differ due to the different thermal expansion coefficients of the interface planes: GaN(0001)/Si(111) and GaN(11–22)/NP–Si(100).

Indeed, the magnitudes of the elastic stresses of the GaN(0001)/Si(111) and GaN(11–22)/NP–Si(113), structures, which occur upon cooling, depend on the difference in the GaN and Si $\Delta\alpha = \alpha_{\text{GaN}} - \alpha_{\text{Si}}$ thermal expansion coefficients for the interface planes. As is known, the thermal expansion coefficients of Si are $k_{\text{Si}} = 3.6 \cdot 10^{-6} \text{ K}^{-1}$ [111], while in GaN, due to crystal anisotropy, the coefficients are different: in the axis direction $\langle a \rangle - k_{\text{GaN}(a)} = 5.6 \cdot 10^{-6} \text{ K}^{-1}$ [136] and $\langle c \rangle - k_{\text{GaN}(c)} = 3.17 \cdot 10^{-6} \text{ K}^{-1}$ [2]. Then, according to [63], the stress arising in the heterostructure due to the difference in thermal stretching coefficients can be estimated from the

expression

$$\sigma_{\Delta\alpha} \approx \frac{E_{\text{GaN}}}{(1 - \nu_{\text{GaN}})} \Delta\alpha \Delta T,$$

where $E_{\text{GaN}} = 295 \text{ GPa}$ and $\nu_{\text{GaN}} = 0.25$, and ΔT — the difference between the epitaxy temperature and room temperature. It is found that the elastic stresses that can occur during cooling of the polar structure are $\sigma_{\Delta\alpha(0001)} = -0.79 \text{ GPa}$; then the stresses that occurred at the epitaxy temperature for the polar structure area $\sigma_{\Delta\alpha(0001)} = -0.33 \text{ GPa}$. Based on the assumption of the equality of the elastic stresses arising at the epitaxy temperature due to the use of Si(111) plane and Si(111) face during nucleation, we determine the value of $\sigma_{\Delta\alpha}$ for the semi-polar structure, which turned out to be equal to -0.34 GPa .

Since the thermal expansion coefficients are currently known only in the $\langle a \rangle$ and $\langle c \rangle$ directions, it is proposed to introduce the effective thermal expansion coefficient of the semi-polar GaN(11–22)-layer on the silicon substrate in the $\langle 11-22 \rangle - k_{\text{GaN}(11-22)}^*$ direction, which should be in the $k_{\text{GaN}(c)} < k_{\text{GaN}(11-22)}^* < k_{\text{GaN}(a)}$ interval (Fig. 26). Obviously, if we put $k_{\text{GaN}(11-22)}^* = 4.47 \cdot 10^{-6} \text{ K}^{-1}$, then the value of $\sigma_{\Delta\alpha(11-22)} = -0.34 \text{ GPa}$ and coincides with the experimentally obtained stress value for the semi-polar layer.

So, the use of nanoscale structured Si(113) substrate in the formation of semi-polar GaN(11–22) layer on the templet leads to lower internal stresses in the semi-polar layer than in the polar on substrate Si(111).

1.2.7. Surface morphology of GaN(11–22)/NP–Si(113), GaN(10–11)/NP–Si(100) on substrates NP–Si(100), NP–Si(113)

During the experiment, semi-polar GaN(11–22) layers on NP–Si(113) and GaN(10–11) on NP–Si(100) and for comparison polar GaN(0001) on flat substrate Si(111) were grown by the MOCVD method under the same temperature and time regimes.

AFM of the layer surface showed a significant difference in the morphology of GaN(0001) layers grown on the flat surface of Si(111) substrate and GaN(10–11)

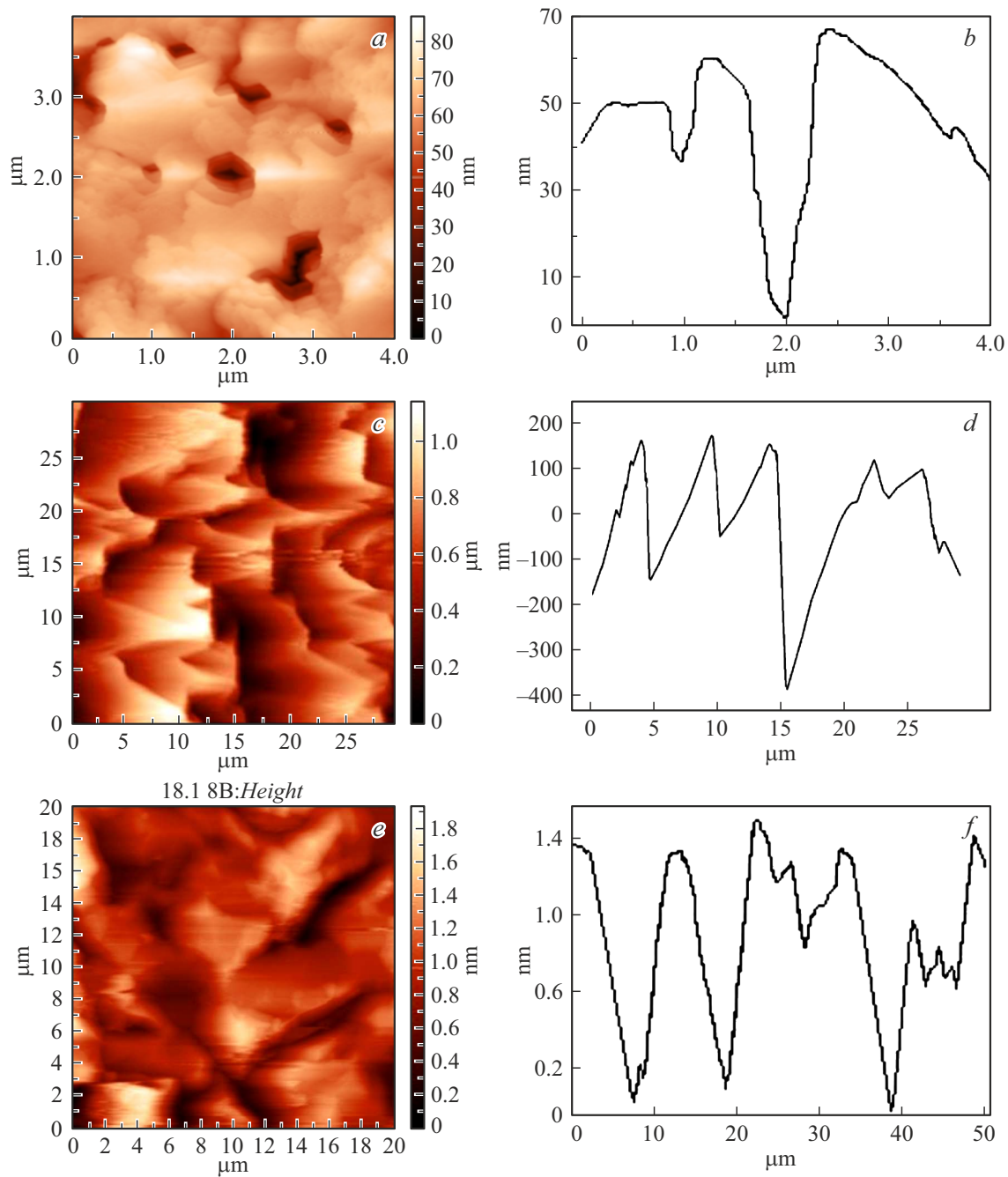


Figure 27. AFM scan images and surface profile of structures: *a, b* — GaN(0001)/Si(111); *c, d* — GaN(10–11)/NP–Si(100); *e, f* — GaN(11–22)/NP–Si(113) [137].

and GaN(11–22) layers obtained on nanostructured NP–Si(100) and NP–Si(113) substrates, respectively. surface of GaN(0001) layer contained defects with depth of around 50 nm, but heterogeneity of the layer on a site $40 \times 40 \mu\text{m}$ made 15 nm max. (Fig. 27, *a, b*). The surface of the GaN(10–11) semi-polar layer had a pronounced asymmetric character inherent in the semi-polar gallium nitride blocks, which arise from the asymmetric properties of the NP–Si(100) substrate, as outlined in [17]. The magnitude of surface inhomogeneity in such structures

over an area of $30 \times 30 \mu\text{m}$ was about 150–200 nm (Fig. 27, *c, d*). It should be noted that when scanned in the direction perpendicular to the grooves, the distance between the hump peaks in the GaN(10–11) layer was 3–5 μm , and on is significantly different from the similar distance given by the substrate NP–Si(100) — less than 100 nm (Fig. 27 *c, d*).

The surface of the semi-polar GaN(11–22) layer, when scanned similarly over an area of $50 \times 50 \mu\text{m}$, had the character of rectangular blocks of size $2 \times 8 \mu\text{m}$, with

sags of up to $1.3\ \mu\text{m}$ observed between them. The distance between the humps in the GaN(11–22) layer was about $10\ \mu\text{m}$ according to AFM data (Fig. 27, *e,f*). Therefore, aspect ratio (height-to-width ratio) of semi-polar gallium nitride blocks is 0.05 for GaN(10–11) and 0.13 for Ga(11–22) (Fig. 27).

In synthesis of gallium nitride, evolution of morphology will depend on the speed of growth depending on orientation of crystal surface faces. As is commonly known, for face (111) any atom adsorbed on this surface will be irreversibly built into the crystal structure. For face (111) the surface growth takes place according to random addition mechanism, and none of the adsorbed atoms is released back into vapor phase [138]. Surfaces with large growth rates often disappear completely, i.e. surfaces with large surface energies will vanish. In a thermodynamically equilibrium crystal, only surfaces with the lowest energies [139] will remain. And this should result in formation of semi-polar GaN(10–11) and GaN(11–22) planes on the surface, if grooves with Si(111) planes are used.

Previously it was noted that in selective gas phase epitaxy growth of GaN from metal-organic compounds on faces of GaN mesa-strips previously formed by local epitaxy in windows Si_3N_4 , if hydrogen is used as carrier gas, occurs mostly in lateral direction. According to experimental results [140], increase in growth temperature results in increased height and decreased diameter in epitaxy in the hydrogen atmosphere, i.e. aspect ratio increases. On the contrary, aspect ratio decreases with temperature growth under conditions of nitrogen as carrier gas [141].

In process of MOCVD you can identify two mechanisms for mass transfer on the surface of the nanostructured substrate: diffusion in a vapor phase and surface diffusion. Molecules are included into epitaxial structure with the same probability in the entire surface area of inclined face of nanostructured Si(100) and Si(113) substrates, if effective length of diffusion exceeds half of the face length. Otherwise, uneven accumulation of epitaxial material will be observed on face tops.

Surface diffusion of Al and Ga adatoms on AlN and GaN surface plays an important role for nucleation and growth of semi-polar layers on patterned substrates. It is known that free path of Al adatom on AlN surface is short and is about $40\ \text{nm}$ [142]. Free path of Ga adatom on GaN surface is different for polar (0001) and semi-polar (10–11) faces of GaN during MOCVD epitaxy and is equal to 1430 and $535\ \text{nm}$, respectively [143]. However, there are reports that the free path length of Ga in hydrogen atmosphere on GaN surface at 1040°C is much longer and can be of the magnitude $15\ \mu\text{m}$ for epitaxy in hydrogen atmosphere [22]. Therefore, epitaxial growth of AlN buffer layer on NP–Si(100) and NP–Si(113) occurs under the conditions, when diffusion length of Al adatom is comparable to size of groove Si(111) face, and this provides for even growth along Si(111) faces. In hydrogen environment diffusion length of Ga adatom is much longer than distance between grooves of nanostructured substrates,

and this results in formation of gallium nitride blocks with large sizes on the substrate. Indeed, from the AFM data (Fig. 27, *d,f*) we can conclude that the sizes of the blocks formed on the surface of NP–Si(100) and NP–Si(113) are close, which can be attributed to the approximately the same diffusion length of Ga atoms, equal to $3\text{--}4\ \mu\text{m}$. Since the tangential growth rate of GaN(10–11) is found to be significantly smaller than that of GaN(11–22), this leads to a different value of the aspect ratio for the semi-polar layers.

Thus, the surface morphology of the semi-polar layers indicates that the higher aspect ratio of GaN(11–22) blocks relative to GaN(10–11) is due to the different growth rate of the semi-polar and polar facets and the higher growth rate of the semi-polar facet of GaN(11–22) compared to GaN(10–11). In general these results demonstrate that morphology of semi-polar layers in epitaxy on a nanostructured surface significantly differs from the conditions of growth on flat polar surfaces.

We note that a combined technique has been proposed to grow high quality semi-polar GaN(11–22) with a smooth surface on a structured Si(113) substrate. First, an AlN layer is grown on the groove wall surface of Si(1–11) to prevent back-etching during Ga melting, then a high-temperature GaN layer is deposited, and finally a low-temperature GaN [144] layer is deposited.

1.2.8. *c*-GaN/NP–Si(100): model of formation and properties

Recently, the synthesis of cubic gallium nitride *c*-GaN on silicon structured Si(100) substrates by MOCVD [145–147] method has received increased attention.

Cubic-modified gallium nitride (*c*-GaN) is a promising material for electronics [147] due to the absence of internal fields. Typically, cubic GaN is grown by epitaxy on GaAs [148], MgO [149], 3C-SiC [150] substrates.

Two models are known to explain the occurrence of cubic modification of GaN during synthesis on structured Si(100) substrate. According to the model proposed in [145], on a Si(100) substrate with V-shaped grooves with a period of about $1\ \mu\text{m}$, GaN synthesis proceeds in the hexagonal (*h*-) phase, which induces a secondary V-shaped groove with two opposite faces (0001). The *h*–*c* phase transition occurs uniformly and simultaneously along the bottom of the entire secondary groove due to the presence of opposing GaN(0001)-facets, and the surface morphology of *c*-GaN nanoparticles is determined by faceting consisting mainly of (11*n*)-orientation.

In the model proposed in [143], it was noted that if the two growth fronts of the *h*-phase merge at the angle 109.5° (i.e., the angle between the two Ga–N bonds in the tetrahedral compound), then the formation of *c*-GaN between the growth boundaries of the hexagonal phase is possible.

The authors [151] proposed a method to form cubic phase GaN on CMOS-compatible Si(100) substrate, in which nanostructured epitaxy is proposed to integrate

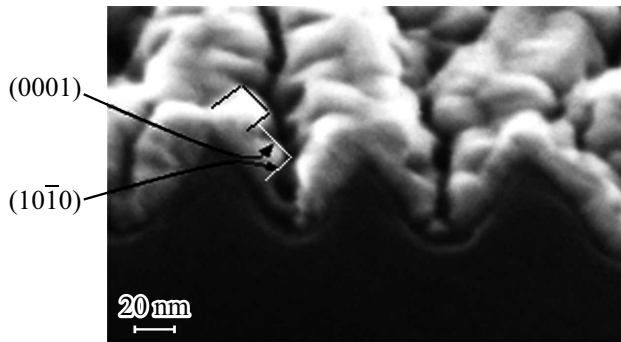


Figure 28. SEM image of the spall and surface of AlN layers with a thickness of about 30 nm synthesized on NP–Si(100)-substrate [152].

stable stress-free *c*-GaN. The results suggest that epitaxial growth conditions and nanostructured pattern parameters are crucial for the preparation of cubic GaN.

We detected a cubic *c*-GaN phase in the synthesis of semi-polar GaN(10–11) on nanostructured silicon — NP–Si(100) substrate and proposed a model which is based on the nucleation of an AlN faceted layer in a nanoscale V-shaped Si(100) groove. The formation of AlN thin layer by MOCVD takes place at low growth rates under groove conditions. Under these growth conditions, AlN nuclei should have facets not only of AlN(0001) but also AlN(10–10). During the subsequent growth of the GaN layer under the conditions of limited diffusion of Ga atoms in the nanowires, the preferred conjugation of the AlN(10–10) and *c*-GaN planes by the „magic mismatch“ mechanism may occur, which leads to the formation of *c*-GaN [152] nuclei.

Scanning electron microscope images of the spall and the surface of the AlN layer show that the layer with a thickness of about 30 nm is formed in the form of crystallites, in which the faces (10–12), (0001) and (10–10) can be distinguished (Fig. 28). It should be noted that the AlN layer has „gorges“ with a transverse dimension of about 10 nm and a depth of about 20–30 nm with facets of AlN(0001) and AlN(10–10) (Fig. 28).

If the synthesis of gallium nitride is carried out at this stage of AlN layer growth, the growth will occur from a very thin gap (~ 10 nm), which leads to the fact that the composition of the V/III gas phase changes strongly from the surface of the AlN layer to the depth of the „gorge“. This creates conditions for gallium nitride nucleation at very low velocities, where Ga adatoms have a choice between nucleating hexagonal *h*-GaN on AlN(0001) faces and cubic *c*-GaN on AlN(10–10) faces. We pose that under conditions of slow nucleation of the GaN layer, the formation of *c*-GaN, conjugated *c* AlN(10–10) crystals partially occurs. This pairing of *f*-germ *c*-GaN with AlN(10–10) may occur by the „magic mismatch“ mechanism when three lattice cells of

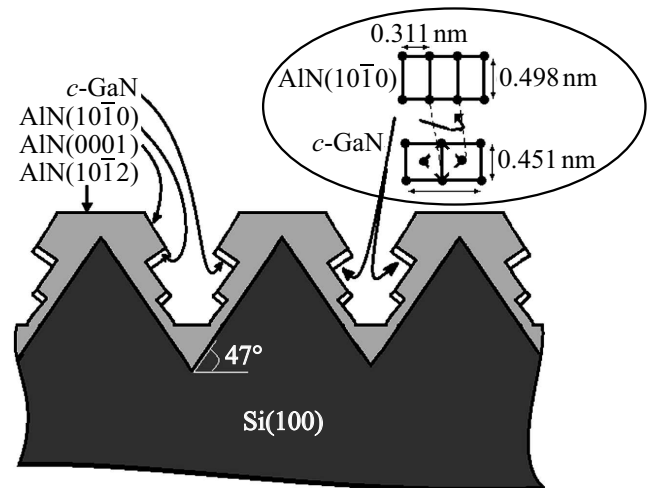


Figure 29. Schematic representation of the nucleation of *c*-GaN (a) and conjugation of *c*-GaN and AlN(10–12) by the mechanism of „magic mismatch“ (b) [152].

AlN(10–10) with two lattice cells of cubic GaN(001) are conjugated. In this case, the mismatch values for the two directions of the AlN(10–10) face are acceptable for value growth

$$f = \frac{3a_{\text{AlN}} - 2a_{\text{GaV}}}{3a_{\text{AlN}}} \approx 3.1\%.$$

It should be noted that the „magic mismatch“ mechanism was used to simulate *c*-GaN epitaxy on a GaAs substrate, where five *c*-GaN(001) atoms are conjugated to four GaAs [153] atoms, where $a_{\text{AlN}} = 0.311$ nm, $a_{\text{AlN}} = 0.498$ nm, $a_{\text{GaV}} = 0.451$ nm.

The luminescence spectra at $T = 80$ K of the GaN layer (Fig. 29) show bands with maxima $h\nu = 3.44$ eV, which we attribute to the interband recombination *c*-GaN, $h\nu = 3.41$ eV, which appears at the occurrence of BSF S-II [45] stacking faults, $h\nu = 3.20$ eV, and $h\nu = 3.16$ eV, which can be attributed to the donor-acceptor recombination radiation of cubic gallium nitride, similar to that in work [146].

So, the luminescence pattern of cubic gallium nitride can be related to the peculiarities of nucleation of GaN layer in „gorges“ of AlN layer arising from nanostructured Si(100) substrate (Fig. 30).

2. Semi-polar GaN-based devices on structured Si substrates

In recent decades, a number of reviews have been published on the growth of gallium nitride layers on silicon substrate orientation (111) [154], the development of power electronic devices based on GaN on Si(111) [155] and the properties of LEDs based on III-nitrides [156]. In work [157], the integration of Si(100) MOSFET and AlGaIn/GaN high electron mobility transistors (HEMTs)

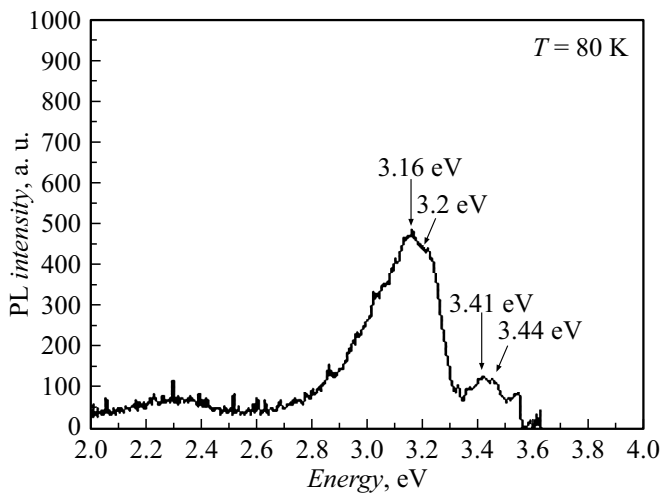


Figure 30. Photoluminescence spectrum of GaN/AlN/NP–Si(100) structure [152].

grown on Si(111) substrate is proposed for the first time. To provide Si(100)–GaN compatible process, the authors fabricated a virtual structure through AlGaN/GaN (HEMT) and Si(100)(MOSFET) bonding and etching technique.

To date, few papers have been published on the application of semi-polar layers synthesized on structured Si substrate. In comparison with publications on the synthesis of semi-polar GaN structures on structured sapphire substrate [36,143,158–163], these works mainly demonstrated a significant reduction of the polarization field in the active areas of semi-polar structures compared to polar [164].

The largest number of publications is devoted to InGaN/GaN(10–11) LED structures. The authors [165] studied InGaN/GaN LEDs with 4-nm-wide active areas fabricated on GaN(10–11)/Si(100)- and GaN(11–22)/Si(113)-layers. Although the LEDs were far from state-of-the-art (e.g., the series resistance was $\sim 100 \Omega$), a dramatic reduction in polarization was confirmed for both semi-polar orientations by the significant reduction in the blue shift of the emission line with increasing current delivery compared to polar LEDs. LEDs based on (11–22) showed more significant emission line broadening at 460 nm than LEDs based on (10–11), suggesting large compositional variations in this orientation. The authors concluded that the orientation (10–11) is preferred for device applications because of the better quality of the layers.

The authors [166,167] reported the optical properties of a 420 nm InGaN/GaN laser structure on GaN(10–11) synthesized on microstrips fabricated on a Si(001) substrate disoriented on 8° . The photoluminescence spectrum observed from the cross section of the sample showed a marked narrowing of the spectrum, indicating the onset of stimulated emission from the active layer on GaN(10–11). The authors [168] observed the generation effect of optical

pumping of InGaN/GaN(10–11) MQW on a structured Si(100) substrate with disorientation 8° .

A group of technologists [169] reported the creation of semi-polar InGaN/GaN(10–11) LEDs with blue and green colors. As expected, the blue semi-polarized LEDs showed only a weak polarization-related wavelength shift at high current densities (4.7 nm in the current density range from 5 to 100 A/cm²). However, green semi-polarized LEDs showed a strong blue shift ~ 100 nm at low current densities, which was attributed to the inhomogeneous formation of layers with high indium content (more than 30%).

The authors [170–172] demonstrated that GaN light-emitting diodes with emission wavelengths of about 530 nm can be synthesized on semi-polar GaN(11–22) grown on structured Si(113) substrates.

The authors [95,173] showed that during HVPE epitaxy of semi-polar layers on templates synthesized by MOCVD, the layer follows the crystal-lattice orientation of the template.

The growth and characterization of a (1011) GaN, InGaN–MQW LED structure grown on structured SOI substrates is reported [174]. Blue LED structures exhibiting a uniform emission wavelength at 450 nm, a crack-free surface, and a roughness of about 5 nm have been fabricated. These results open the way to the fabrication of semi-polar μ LEDs grown on SOI substrates.

Recently [174], it has been reported that GaN/InGaN micro-LEDs (μ LEDs) grown directly on Si with submicron lateral dimensions have been created. The micro-LEDs are fabricated based on an array of N-polar nanowires synthesized by bottom-up selective epitaxy. This research provides new insights and opens a new path for the design, fabrication and integration of high-performance μ LEDs on silicon for a wide range of optical communication applications.

Conclusion

A review of the successes, challenges and prospects of semi-polar wide-band III-nitrides synthesized on structured silicon substrates is presented. It is evident that great success in GaN hetero-epitaxy on sapphire has been achieved in the last two decades. The breakthrough in the demonstration of semi-polar GaN/InGaN(20–21) continuous room-temperature laser diodes on sapphire marks a success in the exploration of high-quality heteroepitaxial semi-polar structures [89]. A laser structure for the ultraviolet emission range was successfully grown on a Si(111) substrate using an AlN/AlGaN multilayer buffer with a step-down of aluminium composition, and the observation of electrically injected generation at room temperature [176] was demonstrated.

Advances in the technology of polar layers on Si(111) and semi-polar layers on sapphire substrates have stimulated the development of heteroepitaxial semi-polar GaN layers on Si(100) and Si(113) substrates. An approach in which

inclined *c*-shaped planes as trench sidewalls are proposed as starting points for GaN growth and, after fusion, eventually lead to semi-polarized layers, looks promising. Interest in semi-polar wide-band III-nitride layers is now evident in a rapidly growing number of publications of results [46,133,144,174] and looks promising for their widespread application in optoelectronics in the near future.

Acknowledgments

The development of technology for semi-polar wide-band III–N layers on silicon substrate has been the main focus of our work for several years. Many of the A.F. Ioffe FTI staff members have contributed to the research mentioned in this review. The authors sincerely thank V.N. Panteleyev, S.N. Rodin, M.P. Shcheglov, and M.E. Kompan for their excellent research in this area and V.K. Smirnov (Quantum Silicon“LLC) for providing nanostructured silicon substrates.

Conflict of interest

The authors declare that they have no conflict of interest.

References

- [1] W.C. Johnson, J.B. Parsons, M.C. Crew. *J. Phys. Chem.*, **36**, 2561 (1932).
- [2] H.P. Maruska, J.J. Tietjen. *Appl. Phys. Lett.*, **15**, 327 (1969).
- [3] H.M. Manasevit, F.M. Erdmann, W.I. Simpson. *J. Electrochem. Soc.*, **118**, 1864 (1971). DOI: 10.1149/1.2407853
- [4] H. Amano, N. Sawaki, I. Akasaki, Y. Toyoda. *Appl. Phys. Lett.*, **48**, 353 (1986). DOI: 10.1063/1.96549
- [5] S. Nakamura, N. Iwasa, M. Senoh, T. Mukai. *Jpn. J. Appl. Phys.*, **31**, 1258 (1992). DOI: 10.1143/JJAP.31.1258
- [6] S. Nakamura, M. Senoh, T. Mukai. *Jpn. J. Appl. Phys.*, **32**, L8 (1993). DOI: 10.1143/JJAP.32.L8
- [7] R.R. Sumathi. *ECS J. Solid State Sci. Technol.*, **10**, 035001 (2021). DOI: 10.1149/2162-8777/abe6f5
- [8] V.Yu. Davydov, A.A. Klochikhin. *Semicond.*, **38** (8), 861 (2004).
- [9] A.E. Romanov, T.J. Baker, S. Nakamura, J.S. Speck. *J. Appl. Phys.*, **100**, 023522 (2006). DOI: 10.1063/1.2218385
- [10] F. Wu, E.C. Young, I. Koslow, M.T. Hardy, P.S. Hsu, A.E. Romanov, S. Nakamura, S.P. DenBaars, J.S. Speck. *Appl. Phys. Lett.*, **99**, 251909 (2011). DOI: 10.1063/1.3671113
- [11] T. Takeuchi, S. Sota, M. Katsuragawa, M. Komori, H. Takeuchi, H. Amano, I. Akasaki. *Jpn. J. Appl. Phys.*, **36**, L382 (1997). DOI: 10.1143/JJAP.36.L382
- [12] D. Rosales, B. Gil, T. Bretagnon, B. Guizal, F. Zhang, S. Okur, M. Monavarian, N. Izyumskaya, V. Avrutin, Ü. Özgür, H. Morkoç, J.H. Leach. *J. Appl. Phys.*, **115**, 073510 (2014). DOI: 10.1063/1.4865959
- [13] W.G. Scheibenzuber, U.T. Schwarz, R.G. Veprek, B. Witzigmann, A. Hangleiter. *Phys. Rev. B*, **80**, 115320 (2009). DOI: 10.1103/PhysRevB.80.115320
- [14] F. Scholz. *Semicond. Sci. Technol.*, **27**, 024002 (2012). DOI: 10.1088/0268-1242/27/2/024002
- [15] T. Wang. *Semicond. Sci. Technol.*, **31**, 093003 (2016). DOI: 10.1088/0268-1242/31/9/093003
- [16] M. Monavarian, A. Rashidi, D. Feezell. *Phys. Status Solidi A*, **216**, 1800628 (2019). DOI: 10.1002/pssa.201800628
- [17] J.E. Northrup. *Appl. Phys. Lett.*, **95**, 133107 (2009). DOI: 10.1063/1.3240401
- [18] T. Takeuchi, H. Amano, I. Akasaki. *Jpn. J. Appl. Phys.*, **39**, 413 (2000). DOI: 10.1143/JJAP.39.413
- [19] S.H. Park. *J. Appl. Phys.*, **91**, 9904 (2002). DOI: 10.1063/1.1480465
- [20] T. Sasaki, S. Zembutsu. *J. Appl. Phys.*, **61**, 2533 (1987). DOI: 10.1063/1.337929
- [21] P. Waltereit, O. Brandt, A. Trampert, H.T. Grahn, J. Menninger, M. Ramsteiner, M. Reiche, K.H. Ploog. *Nature*, **406**, 865 (2000). DOI: 10.1038/35022529
- [22] X. Ni, Y. Fu, Y. T. Moon, N. Biyikli, H. Morkoç. *J. Crystal Growth*, **290**, 166 (2006). DOI: 10.1016/j.jcrysgro.2006.01.008
- [23] Q.S. Paduano, D.W. Weyburne, D.H. Tomich. *J. Cryst. Growth*, **367**, 104 (2013). DOI: 10.1016/j.jcrysgro.2012.12.028
- [24] R. Ravash, J. Blaesing, A. Dadgar, A. Krost. *Appl. Phys. Lett.*, **97**, 142102 (2010). DOI: 10.1063/1.3492835
- [25] F. Ranalli, P.J. Parbrook, J. Bai, K.B. Lee, T. Wang, A.G. Cullis. *Phys. Stat. Sol. C*, **6**, S780 (2009). DOI: 10.1002/pssc.200880948
- [26] K. Okamoto, J. Kashiwagi, T. Tanaka, M. Kubota. *Appl. Phys. Lett.*, **94**, 071105 (2009). DOI: 10.1063/1.3078818
- [27] Y. Enya, Y. Yoshizumi, T. Kyono, K. Akita, M. Ueno, M. Adachi, T. Sumitomo, S. Tokuyama, T. Ikegami, K. Katayama. *Appl. Phys. Express*, **2**, 082101 (2009). DOI: 10.1143/APEX.2.082101
- [28] H. Asamizu, M. Saito, K. Fujito, J.S. Speck, S.P. DenBaars, S. Nakamura. *Appl. Phys. Express*, **1**, 091102 (2008). DOI: 10.1143/APEX.1.091102
- [29] Y. Yoshizumi, M. Adachi, Y. Enya, T. Kyono, S. Tokuyama, T. Sumitomo, K. Akita, T. Ikegami, M. Ueno, K. Katayama. *Appl. Phys. Express*, **2**, 092101 (2009). DOI: 10.1143/APEX.2.092101
- [30] M. Adachi, Y. Yoshizumi, Y. Enya, T. Kyono, T. Sumitomo, S. Tokuyama, S. Takagi, K. Sumiyoshi, N. Saga, T. Ikegami. *Appl. Phys. Express*, **3**, 121001 (2010). DOI: 10.1143/APEX.3.121001
- [31] K.K. Fujito, S. Kubo, I. Fujimura. *MRS Bull.*, **34**, 313 (2009). DOI: 10.1557/mrs2009.92
- [32] H. Masui, S. Nakamura, S.P. DenBaars, U.K. Mishra. *IEEE Trans. Electron Devices*, **57**, 88 (2010). DOI: 10.1109/TED.2009.2033773
- [33] S. Guha, N.A. Bojarczuk. *Appl. Phys. Lett.*, **72**, 415 (1998). DOI: 10.1063/1.120775
- [34] S. Guha, N.A. Bojarczuk. *Appl. Phys. Lett.*, **73**, 1487 (1998). DOI: 10.1063/1.122181
- [35] A.T. Schremer, J.A. Smart, Y. Wang, O. Ambacher, N.C. MacDonald, J.R. Shealy. *Appl. Phys. Lett.*, **76**, 736 (2000). DOI: 10.1063/1.125878
- [36] A. Dadgar. *Physica Status Solidi (b)*, **252**, 1063 (2015). DOI: 10.1002/pssb.201451656
- [37] A. Krost, A. Dadgar. *Mater. Sci. & Engineer. B*, **B93**, 77 (2009). DOI: 10.1016/S0921-5107(02)00043-0
- [38] H. Wang, Z. Lin, W. Wang, G. Li, J. Luo. *J. Alloys and Compounds*, **718**, 28 (2017). DOI: 10.1016/j.jallcom.2017.05.009

- [39] H.R. Shanks, P.D. Maycock, P.H. Sidles, G.C. Danielson. *Phys. Rev.*, **130** (5), 1743 (1963). DOI: 10.1103/PhysRev.130.1743
- [40] M.K. Sunkara, S. Sharma, R. Miranda, G. Lian, E.C. Dickey. *Appl. Phys. Lett.*, **79**, 1546 (2001). DOI: 10.1063/1.1401089
- [41] I. Kim, J. Holmi, R. Raju, A. Haapalinn, S. Suihkonen. *J. Phys. Commun.*, **4**, 045010 (2020). DOI: 10.1088/2399-6528/ab885c
- [42] Y. Zheng, M. Agrawal, N. Dharmarasu, K. Radhakrishnan, S. Patwal. *Appl. Surf. Sci.*, **481**, 319 (2019). DOI: 10.1016/j.apsusc.2019.03.046
- [43] R.G. Banal, M. Funato, Y. Kawakami. *Phys. Status Solidi (c)*, **6**, 599 (2009). DOI: 10.1002/pssc.200880415
- [44] K.-L. Lin, E.-Y. Chang, J.-Ch. Huang, W.-Ch. Huang, Y.-L. Hsiao, Ch.H. Chiang, T. Li, D. Tweet, J.-Sh. Maa, Sh.-T. Hsu. *Phys. Stat. Sol. (c)*, **5** (6), 1536 (2008). DOI: 10.1002/pssc.200778454
- [45] S.L. Selvaraj, A. Watanabe, A. Wakejima, T. Egawa. *IEEE Electron Device Lett.*, **33**, 1375 (2012). DOI: 10.1109/LED.2012.2207367
- [46] N. Wu, N. Wu, Zh. Xing, Sh. Li, L. Luo, F. Zeng, G. Li. *Semicond. Sci. Technol.*, **38**, 063002 (2023). DOI: 10.1088/1361-6641/acca9d
- [47] T. Sasaki, T. Matsuoka. *J. Appl. Phys.*, **77**, 192 (1995). DOI: 10.1063/1.359368
- [48] A. Dadgar, J. Bläsing, A. Diez, A. Alam, M. Heuken, A. Krost. *Jpn. J. Appl. Phys.*, **39**, L1183 (2000). DOI: 10.1143/JJAP.39.L1183
- [49] J. Zhang, X. Yang, Y. Feng, Y. Li, M. Wang, J. Shen, L. Wei, D. Liu, S. Wu, Z. Cai, F. Xu, X. Wang, W. Ge, B. Shen. *Phys. Rev. Materials*, **4**, 073402 (2020). DOI: 10.1103/PhysRevMaterials.4.073402
- [50] Y. Sakai, I. Kawayama, H. Nakanishi, M. Tonouchi. *Scientific Reports*, **5**, 13860 (2015). DOI: 10.1038/srep13860
- [51] S. Bidnyk, B.D. Little, Y.H. Cho, J. Krasinski, J.J. Song, W. Yang, S.A. McPherson. *Appl. Phys. Lett.*, **73**, 2242 (1998). DOI: 10.1063/1.121689
- [52] G.P. Yablonskii, E.V. Lutsenko, V.N. Pavlovskii, V.Z. Zubialevich, A.L. Gurskii, H. Kalisch, A. Szymakowskii, R.A. Jansen, A. Alam, Y. Dikme, B. Schineller, M. Heuken, *Phys. Status Solidi A*, **192**, 54 (2002). DOI: 10.1002/1521-396X(200207)192:1;1-54::AID-PSSA54;3.0.CO;2-2
- [53] B.A. Shuhaimi, H. Kawato, Y. Zhu, T. Egawa. *J. Phys. Conf.*, **152**, 012007 (2009). DOI: 10.1088/1742-6596/152/1/012007
- [54] X. Lu, C. Liu, H. Jiang, X. Zou, A. Zhang, K.M. Lau. *Appl. Phys. Lett.*, **109**, 053504 (2016). DOI: 10.1063/1.4960105
- [55] J. Yuan, W. Cai, X. Gao, G. Zhu, D. Bai, H. Zhu, Y. Wang. *Appl. Phys. Express*, **9**, 032202 (2016). DOI: 10.7567/APEX.9.032202
- [56] W. Cai, X. Gao, W. Yuan, Y. Yang, J. Yuan, H. Zhu, Y. Wang. *Appl. Phys. Express*, **9**, 052204 (2016).
- [57] Y. Wang, G. Zhu, W. Cai, X. Gao, Y. Yang, J. Yuan, Z. Shi, H. Zhu. *Appl. Phys. Lett.*, **108**, 162102 (2016). DOI: 10.1063/1.4947280
- [58] D. Bai, T. Wu, X. Li, X. Gao, Y. Xu, Z. Cao, H. Zhu, Y. Wang. *Appl. Phys. B*, **122**, 9 (2016). DOI: 10.1007/s00340-015-6293-8
- [59] D. Bai, X. Gao, W. Cai, W. Yuan, Z. Shi, X. Li, Y. Xu, J. Yuan, G. Zhu, Y. Yang, C. Yang, X. Cao, H. Zhu, Y. Wang. *Appl. Phys. A*, **122**, 535 (2016). DOI: 10.1007/s00339-016-0075-y
- [60] W. Cai, Y. Yang, X. Gao, J. Yuan, W. Yuan, H. Zhu, Y. Wang. *Opt. Express*, **24**, 6004 (2016). DOI: 10.1364/OE.24.006004
- [61] Y. Jiang, Z. Shi, S. Zhang, J. Yuan, Z. Hu, X. Shen, B. Zhu, Y. Wang. *IEEE Electron Dev. Lett.*, **38**, 1684 (2017). DOI: 10.1109/LED.2017.2760318
- [62] T. Narita, H. Iguchi, K. Horibuchi, N. Otake, S. Hoshi, K. Tomita. *Jpn. J. Appl. Phys.*, **55**, 05FB01 (2016). DOI: 10.7567/JJAP.55.05FB01
- [63] Y. Dai, S. Li, H. Gao, W. Wang, Q. Sun, Q. Peng, C. Gui, Z. Qian, S. Liu. *J. Mater. Sci: Mater. Electron.*, **27**, 2004 (2016). DOI: 10.1007/s10854-015-3984-1
- [64] E. Valcheva, J. Birch, P.O.A. Persson, S. Tungasmita, L. Hultman. *J. Appl. Phys.*, **100** (12), 123514 (2006). DOI: 10.1063/1.2402971
- [65] A. Dadgar, F. Schulze, M. Wienecke, A. Gadanez, J. Bläsing, P. Veit, T. Hempel, A. Diez, J. Christen, A. Krost. *New J. Physics*, **9**, 389 (2007). DOI: 10.1088/1367-2630/9/10/389
- [66] X. Zhang, Y.-T. Hou, Z.-C. Feng, J.L. Chen. *J. Appl. Phys.*, **89** (11), 6165 (2001). DOI: 10.1063/1.1368162
- [67] A.M. Aseev (ed.). *Atomnaya struktura poluprovodnikovyykh sistem* (Novosibirsk: SB RAS, 2006), p. 292.
- [68] V. Lebedev, J. Jinschek, J. Kräußlich, U. Kaiser, B. Schröter, W. Richter. *J. Cryst. Growth*, **230** (3), 426 (2001). DOI: 10.1016/S0022-0248(01)01241-6
- [69] V.N. Bessolov, E.V. Gushchina, E.V. Konenkova, T.V. L'vova, V.N. Pantelev, M.P. Shcheglov. *Tech. Phys. Letters*, **44** (1), 81 (2018). DOI: 10.1134/S106378501801011X.
- [70] W.K. Wang, M.-C. Jiang. *Jpn. J. Appl. Phys.*, **55**, 095503 (2016). DOI: 10.7567/JJAP.55.095503
- [71] J.-C. Gerbedoen, A. Soltani, S. Joblot, J.-C. De Jaeger, Ch. Gaquière, Y. Cordier, F. Semond. *IEEE Transactions on Electron Devices*, **57** (7), 1497 (2010). DOI: 10.1109/TED.2010.2048792
- [72] S.T. Kim, Y.J. Lee, S.H. Chung, D.C. Moon. *J. Korean Phys. Soc.*, **33**, S313 (1998)
- [73] F. Schulze, A. Dadgar, J. Bläsing, A. Krost. *Appl. Phys. Lett.*, **84** (23), 4747 (2004). DOI: 10.1063/1.1760214
- [74] V.N. Bessolov, E.V. Gushchina, E.V. Konenkova, S.D. Konenkov, T.V. L'vova, V.N. Pantelev, M.P. Shcheglov. *Tech. Phys.*, **64** (4), 531 (2019). DOI: 10.1134/S1063784219040054
- [75] V.N. Bessolov, Y.V. Zhilyaev, E.V. Konenkova, N.K. Poletaev, S. Sharofidinov, M.P. Shcheglov. *Tech. Phys. Lett.*, **38** (1), 9 (2012). DOI: 10.1134/S1063785012010051
- [76] V.N. Bessolov, E.V. Konenkova, S.A. Kukushkin, A.V. Osipov, S.N. Rodin. *Rev. Adv. Mater. Sci.*, **38**, 75 (2014).
- [77] V. Bessolov, A. Kalmykov, S. Konenkov, E. Konenkova, S. Kukushkin, A. Myasoedov, A. Osipov, V. Pantelev. *Microelectron. Eng.*, **178**, 34 (2017). DOI: 10.1016/j.mee.2017.04.047
- [78] H.-J. Lee, S.-Y. Bae, K. Lekhal, A. Tamura, T. Suzuki, M. Kushimoto, Y. Honda, H. Amano. *J. Cryst. Growth*, **468**, 547 (2016). DOI: 10.1016/j.jcrysgro.2016.11.116
- [79] R. Ravash, J. Bläsing, T. Hempel, M. Noltemeyer, A. Dadgar, J. Christen, A. Krost. *Appl. Phys. Lett.*, **95**, 242101 (2009). DOI: 10.1063/1.3272673
- [80] S.A. Kukushkin, A.V. Osipov. *J. Appl. Phys.*, **113**, 024909 (2013). DOI: 10.1063/1.4773343
- [81] V.N. Bessolov, Y.V. Zhilyaev, E.V. Konenkova, S.N. Rodin, N.V. Seredova, N.A. Feoktistov, M.P. Shcheglov, A.A. Efimov,

- S.A. Kukushkin, A.V. Osipov. Russian Chemical Journal, **57** (6), 133 (2013).
- [82] V. Bessolov, A. Kalmykov, E. Konenkova, S. Kukushkin, A. Myasoedov, N. Poletaev, S. Rodin. J. Cryst. Growth, **457**, 202 (2017). DOI: 10.1016/J.JCRYSGRO.2016.05.025
- [83] D.V. Dinh, S. Presa, M. Akhter, P.P. Maaskant, B. Corbett, P.J. Parbrook. Semicond. Sci. Technol., **30**, 125007 (2015). DOI: 10.1088/0268-1242/30/12/125007
- [84] D.V. Dinh, P.J. Parbrook. J. Cryst. Growth, **501**, 34 (2018). DOI: 10.1016/j.jcrysgro.2018.08.021
- [85] T. Isshiki, K. Nishio, Y. Abe, J. Komiyama, S. Suzuki, H. Nakanishi. Mater. Scien. Forum, **600–603**, 1317 (2009). DOI: 10.4028/www.scientific.net/MSF.600-603.1317
- [86] Y. Abe, J. Komiyama, T. Isshiki, S. Suzuki, A. Yoshida, H. Ohishi, H. Nakanishi. Mater. Scien. Forum, **600–603**, 1281 (2009). DOI: 10.4028/www.scientific.net/MSF.600-603.1281
- [87] V.N. Bessolov, E.V. Konenkova, S.A. Kukushkin, V.I. Nikolaev, A.V. Osipov, S. Sharofidinov, M.P. Shcheglov. Tech. Phys. Lett., **39** (3), 274 (2013). DOI: 10.1134/S106378501303019X
- [88] A.A. Koryakin, S.A. Kukushkin, A.V. Osipov, S.Sh. Sharofidinov, M.P. Shcheglov. Materials, **15** (18), 6202 (2022). DOI: 10.3390/ma15186202
- [89] H. Li, H. Zhang, J. Song, P. Li, Sh. Nakamura, S.P. DenBaars. Appl. Phys. Rev., **7**, 041318 (2020). DOI: 10.1063/5.0024236
- [90] T. Mitsunari, H.J. Lee, Y. Honda, H. Amano. J. Cryst. Growth, **431**, 60 (2015). DOI: 10.1016/j.jcrysgro.2015.08.027
- [91] Y. Honda, N. Kameshiro, M. Yamaguchi, N. Sawaki. J. Cryst. Growth, **242** (1), 82 (2002). DOI: 10.1016/S0022-0248(02)01353-2
- [92] R.A. Wind, M.A. Hines. Surf. Science, **460**, 21 (2000). DOI: 10.1016/S0039-6028(00)00479-9
- [93] V.K. Smirnov, D.S. Kibalov, O.M. Orlov, V.V. Graboshnikov. Nanotechnology, **14**, 709 (2003). DOI: 10.1088/0957-4484/14/7/304
- [94] V.N. Bessolov, M.E. Kompan, E.V. Konenkova, V.N. Pantelev. Tech. Phys. Lett., **46** (1), 59 (2020). DOI: 10.1134/S1063785020010174
- [95] L. Zhang, J. Wu, F. Liu, T. Han, X. Zhu, M. Li, Q. Zhao, T.J. Yu. Cryst. Eng. Comm., **23**, 3364 (2021). DOI: 10.1039/D1CE00040C
- [96] T. Liu, J. Zhang, X. Su, J. Huang, J. Wang, K. Xu. Sci. Rep., **6**, 26040 (2016). DOI: 10.1038/srep26040
- [97] L. Huang, Y. Li, W. Wang, X. Li, Y. Zheng, H. Wang, G. Li. Appl. Surf. Science, **435**, 163 (2018). DOI: 10.1016/j.apsusc.2017.11.002
- [98] V.N. Bessolov, E.V. Konenkova, S.N. Rodin, D.S. Kibalov, V.K. Smirnov. Semiconductors, **55** (4), 471 (2021). DOI: 10.1134/S1063782621040035
- [99] R.G. Banal, M. Funato, Y. Kawakami. Phys. Status Solidi C, **6** (2), 599 (2009). DOI: 10.1002/pssc.200880415
- [100] T. Szymanski, M. Wosko, B. Paszkiewicz, B. Paszkiewicz, R. Paszkiewicz. J. Vac. Sci. & Technol. A: Vacuum, Surfaces, and Films, **34**, 051504 (2016). DOI: 10.1116/1.4958805
- [101] V.N. Bessolov, E.V. Konenkova, T.A. Orlova, S.N. Rodin, M.P. Shcheglov, D.S. Kibalov, V.K. Smirnov. Tech. Phys. Lett., **44** (6), 525 (2018). DOI: 10.1134/S1063785018060172
- [102] B. Ma, D. Jinno, H. Miyake, K. Hiramatsu, H. Harima. Appl. Phys. Lett., **100**, 011909 (2012). DOI: 10.1063/1.3674983
- [103] M. Kuball, J.M. Hayes, A.D. Prins, N.W.A. van Uden, D.J. Dunstan, Ying Shi, J.H. Edgar. Appl. Phys. Lett., **78**, 724 (2001). DOI: 10.1063/1.1344567
- [104] V.N. Bessolov, M.E. Kompan, E.V. Konenkova, S.N. Rodin. Bull. RAS: Physics, **86** (7), 817 (2022). DOI: 10.3103/S1062873822070103
- [105] P. Perlin, A. Polian, T. Suski. Physical Review B, **47** (5), 2874 (1993). DOI: 10.1103/PhysRevB.47.2874
- [106] V.N. Bessolov, E.V. Konenkova, V.N. Pantelev. Tech. Phys., **65** (12), 2031 (2020). DOI: 10.1134/S1063784220120051
- [107] C.E. Dreyer, A. Janotti, C.G. Van de Walle. Appl. Phys. Lett., **106**, 212103 (2015). DOI: 10.1063/1.4921855
- [108] E.V. Etzkom, D.R. Clarke. J. Appl. Phys., **89** (2), 1025 (2001). DOI: 10.1063/1.1330243
- [109] Sh.-R. Jian, J.-Y. Juang. J. Nanomaterials, **2012**, 914184 (2012). DOI: 10.1155/2012/914184
- [110] P.R. Tavernier, B. Imer, S.P. DenBaars, D.R. Clarke. Appl. Phys. Lett., **85** (20), 4630 (2004). DOI: 10.1063/1.1818736
- [111] W.M. Vim, R.J. Paff. J. Appl. Phys., **45**, 1456 (1974). DOI: 10.1063/1.1663432
- [112] A.M. Smirnov, E.C. Young, V.E. Bougrov, J.S. Speck, A.E. Romanov. J. Appl. Phys., **126**, 245104 (2019). DOI: 10.1063/1.5126195
- [113] G.-T. Chen, S.-P. Chang, J.-I. Chyi, M.-N. Chang. Appl. Phys. Lett., **92**, 241904 (2008). DOI: 10.1063/1.2946655
- [114] M.E. Bachlechner, A. Omeltchenko, A. Nakano, R.K. Kalia, P. Vashista. Phys. Rev. Lett., **84**, 322 (2000). DOI: 10.1103/PhysRevLett.84.322
- [115] T. Akiyama, Y. Seta, K. Nakamura, T. Ito. Phys. Rev. Mater., **3**, 023401 (2019). DOI: 10.1103/PhysRevMaterials.3.023401
- [116] T. Kawamura, T. Akiyama, A. Kitamoto, M. Imanishi, M. Yoshimura, Y. Mori, Y. Morikawa, Y. Kangawa, K. Kakimoto. J. Cryst. Growth, **549**, 125868 (2020). DOI: 10.1016/j.jcrysgro.2020.125868
- [117] V. Bessolov, A. Zubkova, E. Konenkova, S. Konenkov, S. Kukushkin, T. Orlova, S. Rodin, V. Rubets, D. Kibalov, V. Smirnov. Phys. Status Solidi B, **256** (2), 1800268 (2019). DOI: 10.1002/pssb.201800268
- [118] J. Lähnemann, U. Jahn, O. Brandt, T. Flissikowski, P. Dogan, H.T. Grahm. J. Phys. D: Appl. Phys., **47**, 423001 (2014). DOI: 10.1088/0022-3727/47/42/423001
- [119] P. Vennégués, J.M. Chauveau, Z. Bougrioua, T. Zhu, D. Martin, N. Grandjean. J. Appl. Phys., **112**, 113518 (2012). DOI: 10.1063/1.4768686
- [120] W. Rieger, R. Dimitrov, D. Brunner, E. Rohrer, O. Ambacher, M. Stutzmann. Phys. Rev. B, **54**, 17596 (1996). DOI: 10.1103/PhysRevB.54.17596
- [121] V.N. Bessolov, E.V. Konenkova, T.A. Orlova, S.N. Rodin, N.V. Sereдова, A.V. Solomnikova, M.P. Shcheglov, D.S. Kibalov, V.K. Smirnov. Semicond., **53** (7), 989 (2019). DOI: 10.1134/S1063782619070054
- [122] V.N. Bessolov, E.V. Konenkova, S.A. Kukushkin, A.V. Osipov, S.N. Rodin. Rev. Adv. Mater. Sci., **38** (1), 75 (2014).
- [123] V.N. Bessolov, E.V. Konenkova, S.N. Rodin. FTP, **57**, 1 (3) (2023). (in Russian). DOI: 10.21883/FTP.2023.01.54923.3994
- [124] B.K. Vainstein, A.A. Chernov, L.A. Shuvalov (eds.). *Sovremennaya kristallografiya. Vol. 3. Obrazovaniye kristallov* (M. Nauka, 1980), p. 408.
- [125] I. Sunagawa. *Crystals Growth, Morphology and Perfection* (Cambridge University Press, NY, USA, 2005)

- [126] Razia, M. Chugh, M. Ranganathan. *Appl. Surf. Science*, **566**, 150627 (2021). DOI: 10.1016/j.apsusc.2021.150627
- [127] S. Washiyama, P. Reddy, F. Kaess, R. Kirste, S. Mita, R. Collazo, Z. Sitar. *J. Appl. Phys.* **124**, 115304 (2018). DOI: 10.1063/5.0002891
- [128] P. Reddy, S. Washiyama, F. Kaess, R. Kirste, S. Mita, R. Collazo, Z. Sitar. *J. Appl. Phys.*, **122**, 245702 (2017). DOI: 10.1063/1.5002682
- [129] K. Wang, R. Kirste, S. Mita, S. Washiyama, W. Mecouch, P. Reddy, R. Collazo, Z. Sitar. *Appl. Phys. Lett.*, **120**, 032104 (2022); DOI: 10.1063/5.0077628
- [130] X. Yu, Y. Hou, S. Shen, J. Bai, Y. Gong, Y. Zhang, T. Wang. *Phys. Status Solidi C*, **13**(5–6), 190 (2016). DOI: 10.1002/pssc.201510209
- [131] J. Bai, X. Yu, Y. Gong, Y.N. Hou, Y. Zhang, T. Wang. *Semicond. Sci. Technol.*, **30**, 065012 (2015). DOI: 10.1088/0268-1242/30/6/065012
- [132] Y. Cai, X. Yu, S. Shen, X. Zhao, L. Jiu, C. Zhu, T. Wang. *Semicond. Sci. Technol.*, **34**(4), 045012 (2019). DOI: 10.1088/1361-6641/ab08bf
- [133] B. Mao, S. Xing, G. Zhao, L. Wang, N. Zhang, H. Du, G. Liu. *Semicond. Sci. Technol.*, to be published (27.01.2023).
- [134] M. Houry, M. Leroux, M. Nemoz, G. Feuillet, J. Zúñiga-Pérez, P. Vennégués. *J. Cryst. Growth*, **419**, 88 (2015). DOI: 10.1016/j.jcrysgro.2015.02.098
- [135] X. Yu. *MOCVD Growth of Novel GaN Materials on Silicon Substrates*, A thesis submitted for the degree of Doctor of Philosophy (Ph.D.) (The University of Sheffield, Faculty of Engineering Department of Electronic and Electrical Engineering, January, 2017).
- [136] W. Qian, M. Skowronski, G.R. Rohrer. *MRS. Online Proceed. Library*, **423**, 475 (1996). DOI: 10.1557/PROC-423-475
- [137] V.N. Bessolov, E.V. Konenkova, T.A. Orlova, S.N. Rodin, A.V. Solomnikova. *Tech. Phys.*, **67**(5), 609 (2022). DOI: 10.21883/TP.2022.05.53677.12-22
- [138] P. Hartman, W.G. Perdok. *Acta Cryst.*, **8**, 49 (1955). DOI: 10.1107/S0365110X55000121
- [139] W.W. Mullins. *Metal Surfaces: Structure, Energetics and Kinetics* (The American Society of Metals, Metals Park, OH, 1962)
- [140] B.-O. Jung, S.-Y. Bae, Y. Kato, M. Imura, D.-S. Lee, Y. Honda, H. Amano. *Cryst. Eng. Comm.*, **16**, 2273 (2014). DOI: 10.1039/C3CE42266F
- [141] M. Nami, R. Eller, S. Okur, A. Rishinaramangalam, S. Liu, I. Brener, D. Feezell. *Nanotechnology*, **28**, 025202 (2017). DOI: 10.1088/0957-4484/28/2/025202
- [142] C. Bayram, J.A. Ott, K.-T. Shiu, Ch.-W. Cheng, Y. Zhu, J. Kim, M. Razeghi, D.K. Sadana. *Adv. Funct. Mater.*, **24**(28), 4492 (2014). DOI: 10.1002/adfm.201304062
- [143] T. Narita, T. Hikosaka, Y. Honda, M. Yamaguchi, N. Sawaki. *Phys. Stat. Sol. C*, **0**(7), 2154 (2003). DOI: 10.1002/pssc.200303511
- [144] B. Mao, Sh. Xing, G. Zhao, L. Wang, N. Zhang, H. Du, G. Liu. *Semicond. Sci. Technol.*, **38**, 035014 (2023). DOI: 10.1088/1361-6641/acb6ad
- [145] S.C. Lee, Y.-B. Jiang, M.T. Durniak, T. Detchprohm, C. Wetzel, S.R.J. Brueck. *Cryst. Growth Des.*, **16**, 2183 (2016). DOI: 10.1021/acs.cgd.5b01845
- [146] R. Liu, R. Schaller, Ch.Q. Chen, C. Bayram. *ACS Photonics*, **5**(3), 955 (2018). DOI: 10.1021/acsp Photonics.7b01231
- [147] S.C. Lee, Y.-B. Jiang, M. Durniak, C. Wetzel, S.R.J. Brueck. *Nanotechnology*, **30**, 025711 (2019). DOI: 10.1088/1361-6528/aae9a2
- [148] D.J. As, A. Richter, J. Bush, M. Lubbers, J. Mimkes, K. Lischka. *Appl. Phys. Lett.*, **76**, 13 (2000). DOI: 10.1557/PROC-639-G5.9
- [149] V.D.C. Garcia, I.E.O. Hinoztroza, A.E. Echavarría, E.L. Luna, A.G. Rodríguez, M.A. Vidal. *J. Cryst. Growth*, **418**, 120 (2015). DOI: 10.1016/j.jcrysgro.2015.02.033
- [150] C.H. Wei, Z.Y. Xie, L.Y. Li, Q.M. Yu, J.H. Edgar, J. Electron. Mater., **29**(3), 317 (2000). DOI: 10.1007/s11664-000-0070-z
- [151] C. Bayram, J.A. Ott, K.-T. Shiu, C.-W. Cheng, Y. Zhu, J. Kim, M. Razeghi, D.K. Sadana. *Adv. Funct. Mater.*, **24**(28), 4492 (2014). DOI: 10.1002/adfm.201304062
- [152] V. Bessolov, E. Konenkova, S. Kononkov, S. Rodin, N. Seredova. *J. Phys.: Conf. Ser.*, **1697**(1), 012099 (2020). DOI: 10.1088/1742-6596/1697/1/012099
- [153] K.H. Plog, O. Brandt, H. Yang, B. Yang, A. Trampert. *J. Vac. Sci. Technol.*, **16**, 2229 (1998). DOI: 10.1116/1.590153
- [154] A.S. Bakri, N. Nayan, A.Sh.A. Bakar, M. Tahan, N.A. Raship, W.H.A. Majid, M.K. Ahmad, S.Ch. Fhong, M.Z. Sahdan, M.Y. Ahmad. *Intern. J. Nanoelectron. Mater.*, **13**(1), 199 (2020).
- [155] Y. Zhong, J. Zhang, Sh. Wu, L. Jia, X. Yang, Y. Liu, Y. Zhang, Q. Sun. *Fundamental Research*, **2**, 462 (2021). DOI: 10.1016/j.fmre.2021.11.028
- [156] Th.A. Tabbakh, D. Anandan, M.J. Sheldon, P. Tyagi, A. Alfaifi. *Recent Advancements in GaN LED Technology* (IntechOpen, 2022). DOI: 10.5772/intechopen.107365
- [157] J.W. Chung, J.-K. Lee, E.L. Piner, T. Palacios. *IEEE Electron Device Lett.*, **30**(10), 1015 (2009). DOI: 10.1109/led.2009.2027914
- [158] H. Furuya, N. Okada, K. Tadatomo. *Phys. Stat. Sol. C*, **9**, 568 (2012). DOI: 10.1002/pssc.201100352
- [159] H. Furuya, Y. Hashimoto, K. Yamane, N. Okada, K. Tadatomo. *J. Cryst. Growth*, **391**, 41 (2014). DOI: 10.1016/j.jcrysgro.2013.12.032
- [160] P. de Mierry, L. Kappei, F. Tendille, P. Vennégués, M. Leroux, J. Zuniga-Perez. *Phys. Stat. Sol. B*, **253**, 105 (2016). DOI: 10.1002/pssb.201552298
- [161] N. Okada, A. Kurisu, K. Murakami, K. Tadatomo. *Appl. Phys. Express*, **2**, 091001 (2009). DOI: 10.1143/apex.2.091001
- [162] F. Tendille, P. De Mierry, P. Vennégués, S. Chenot, M. Teisseire. *J. Cryst. Growth*, **404**, 177 (2014). DOI: 10.1016/j.jcrysgro.2014.07.020
- [163] N. Okada, K. Uchida, S. Miyoshi, K. Tadatomo. *Phys. Stat. Sol. A*, **209**, 469 (2012). DOI: 10.1002/pssa.201100385
- [164] K. Ding, V. Avrutin, N. Izyumskaya, S. Metzner, F. Bertrambr J. Christen, U. Ozgur, H. Morkoc. *Proc. SPIE*, 10532, Gallium Nitride Materials and Devices XIII, 1053208 (2018). DOI: 10.1117/12.2291281
- [165] T. Hikosaka, T. Tanikawa, Y. Honda, M. Yamaguchi, N. Sawaki. *Phys. Status Solidi C*, **5**, 2234 (2008). DOI: 10.1002/pssc.200779236
- [166] T. Murase, T. Tanikawa, Y. Honda, M. Yamaguchi, H. Amano. *Phys. Status Solidi C*, **8**(7–8), 2160 (2011). DOI: 10.1002/pssc.201000990
- [167] T. Tanikawa, T. Sano, M. Kushimoto, Y. Honda, M. Yamaguchi, H. Amano. *Japanese Journal of Applied Physics*, **52**, 08JC05 (2013). DOI: 10.7567/JJAP.52.08JC05

- [168] M. Kushimoto, T. Tanikawa, Y. Honda, H. Amano. Appl. Phys. Express, **8**, 022702 (2015). DOI: 10.7567/APEX.8.022702
- [169] B. Reuters, J. Strate, A. Wille, M. Marx, G. Lükens, L. Heuken, M. Heuken, H. Kalisch, A. Vescan. J. Phys. D: Appl. Phys., **48**, 485103 (2015). DOI: 10.1088/0022-3727/48/48/485103
- [170] S. Shen, X. Zhao, X. Yu, C. Zhu, J. Bai, T. Wang. Phys. Status Solidi A, **217**, 1900654 (2020). DOI: 10.1002/pssa.201900654
- [171] X. Yu, Y. Hou, S. Shen, J. Bai, Y. Gong, Y. Zhang, T. Wang. Phys. Status Solidi C, **13**(5–6), 190 (2016). DOI: 10.1002/pssc.201510209
- [172] X. Zhao, K. Huang, J. Bruckbauer, S. Shen, C. Zhu, P. Fletcher, P. Feng, Y. Cai, J. Bai, C. Trager-Cowan, R.W. Martin, T. Wang. Scientific Reports, **10**, 12650 (2020). DOI: 10.1038/s41598-020-69609-4
- [173] V.N. Bessolov, M.E. Kompan, E.V. Konenkova, V.N. Panteleev, S.N. Rodin, M.P. Shcheglov. Tech. Phys. Lett., **45**(6), 529 (2019). DOI: 10.1134/S106378501906004X
- [174] B. Wannous, P.-M. Coulon, L. Dupré, F. Rol, N. Rochat, J. Zuniga-Perez, P. Vennégués, G. Feuillet, F. Templier. Phys. Status Solidi B, 2200582 (2023). DOI: 10.1002/pssb.202200582
- [175] Y. Wu, Y. Xiao, I. Navid, K. Sun, Y. Malhotra, P. Wang, D. Wang, Y. Xu, A. Pandey, M. Reddeppa, W. Shin, J. Liu, J. Min, Z. Mi. Light Sci. Appl., **11**, 294 (2022). DOI: 10.1038/s41377-022-00985-4
- [176] M. Feng, Z. Li, J. Wang, R. Zhou, Q. Sun, X. Sun, D. Li, H. Gao, Y. Zhou, Sh. Zhang, D. Li, L. Zhang, J. Liu, H.-B. Wang, M. Ikeda, X. Zheng, H. Yang. ACS Photonics, **5**(3), 699 (2018). DOI: 10.1021/acsp Photonics.7b01215

Translated by Y.Deineka